

Kinetics of D/H isotope fractionation between molecular hydrogen and water

Nicholas J. Pester^{a, b, *}, Mark E. Conrad^a, Kevin G. Knauss^a, Donald J. DePaolo^{a, b}

^a Earth and Environmental Sciences Area, Lawrence Berkeley National Laboratory, Berkeley, CA 94720, USA

^b Department of Earth and Planetary Science, University of California, Berkeley, Berkeley, CA 94720, USA

*corresponding email: njpester@lbl.gov

ABSTRACT

At equilibrium, the D/H isotope fractionation factor between H₂ and H₂O ($\alpha_{\text{H}_2\text{O-H}_2(\text{eq})}$) is a sensitive indicator of temperature, and has been used as a geothermometer for natural springs and gas discharges. However, $\delta\text{D}_{\text{H}_2}$ measured in spring waters may underestimate subsurface temperatures of origin due to partial isotopic re-equilibration during ascent and cooling. We present new experimental data on the kinetics of D–H exchange for H₂ dissolved in liquid water at temperatures below 100 °C. Comparing these results with published exchange rates obtained from gas phase experiments (100–400 °C), we derive a consistent activation energy of 52 kJ/mol, and the following rate expressions;

$$\ln k = 9.186 - 6298 / T \quad \text{and} \quad k_1 = [\text{H}_2\text{O}] 9764.61 * \exp(-6298 / T)$$

where T is absolute temperature (K), k is the universal rate constant ([L/mol]/hr), and k_1 is a pseudo-first-order constant (hr⁻¹) applicable to water-dominated terrestrial systems by constraining [H₂O] as the density of H₂O (in mol/L) at the P - T of interest. The density-dependent rate constant accounts for the kinetic disparity of D–H exchange with H₂ when dissolved in liquid H₂O relative to a gas/steam phase, exemplified by $1/k_1$ at 100 °C of ~2 days in liquid, versus ~7 yrs in saturated steam. This difference may explain the high variability of $\delta\text{D}_{\text{H}_2}$ observed in fumarolic gases. Fluids convecting in the crust frequently reach $T > 225$ °C, where isotopic equilibrium is rapidly attained (< 1 hr). We compare fractionation factors measured in natural fluids (α_{OBS}) with values expected for equilibrium at the T of acquisition. Where these values differ, we use kinetic models to estimate cooling rates during upward advection that account for the observed disequilibrium. Models fit to fluids from Yellowstone Park and the Lost City (deep-sea) vent field, both recovered at ~90 °C, require respective transit times of ~7 hrs and ~11 days between higher temperature reaction zones and the surface. Using estimates of subsurface depths of origin, however, suggests similar mean fluid flow rates (10s of meters / hr). Additional complications must be considered when interpreting the $\delta\text{D}_{\text{H}_2}$ of lower-temperature effluent. When applied to data from

33 deep-sea hydrothermal systems, our kinetic models indicate microbial catalysis accelerates D–H exchange
34 once fluids cool below ~60 °C. The H₂ measured in both continental alkaline springs and fracture fluids
35 from Precambrian shield rock is likely produced at $T < 100$ °C, through processes such as
36 serpentinization. In these settings, δD_{H_2} values appear closer to equilibrium with H₂O than those from
37 geothermal systems. Considering kinetic isotope effects may yield H₂ that is out of equilibrium when
38 generated at lower temperatures, we calculate maximum (isothermal) times to apparent isotopic
39 equilibrium of 1.3 yrs at 50 °C, 9 yrs at 25 °C, and 35 yrs at 10 °C. A similar calculation applied to
40 Antarctic brines (-13 °C), where measured δD_{H_2} is far from equilibrium, yields ~350 yrs. This time is
41 shorter than the fluids have been isolated (2.8 ka), suggesting kinetic isotope effects associated with H₂
42 destruction or loss via diffusion may also be possible.

43

44 1. INTRODUCTION

45

46 Molecular hydrogen (H₂) is a common component of crustal fluids and discharges, where water
47 has reacted with reduced (usually Fe-bearing) minerals. The concentration of H₂ in volcanic gases and
48 hydrothermal fluids is a function of both temperature (T) and the oxidation state of coexisting mineral
49 assemblages (Chiodini and Marini, 1998; D'Amore and Panichi, 1980; Giggenbach, 1987; Giggenbach,
50 1997; Kishima, 1989; Kishima and Sakai, 1984; Seyfried et al., 1991). Similarly, mafic silicate minerals
51 are unstable in the presence of H₂O at $T < \sim 400$ °C, and partial oxidation of the Fe(II) component is
52 capable of producing significant amounts of H₂ during serpentinization (Berndt et al., 1996a; Klein et al.,
53 2015; Mayhew et al., 2013; McCollom et al., 2016; Seyfried et al., 2007; Sleep et al., 2004).
54 Serpentinization is the most likely source of H₂-rich fluids/gases recovered from alkaline springs,
55 ophiolites, and continental wells at relatively low temperatures ($< \sim 60$ °C) (Abrajano et al., 1990; Barnes
56 et al., 1978; Coveney et al., 1987; Kelley et al., 2005; Neal and Stanger, 1983; Sherwood Lollar et al.,
57 1993b).

58 Hydrogen concentrations measured in natural solutions generally give ambiguous information
59 regarding temperatures of origin or formation. However, isotope fractionation between H₂ and H₂O is not
60 concentration-dependent, and is a less equivocal indicator of temperature. The heavy stable isotope of
61 hydrogen (²H, ~0.015 % of natural abundance) is commonly referred to as deuterium (or D), and the D/H
62 isotope fractionation factor (α) between coexisting H₂O and H₂ is written as;

63

$$64 \alpha_{H_2O-H_2} = [D/H]_{H_2O} / [D/H]_{H_2} = (\delta D_{H_2O} + 10^3) / (\delta D_{H_2} + 10^3) \quad (1)$$

65

66 where $[D/H]$ is the atomic ratio of the heavy and light hydrogen isotopes for each species. In order to
67 facilitate inter-laboratory comparison of results, laboratory measurements of isotopic ratios are usually
68 reported relative to the measured value of an accepted standard (δ notation) such that, for example, δD_{H_2}
69 = $[(D/H)_{H_2} / (D/H)_{\text{standard}} - 1] * 10^3$ (Craig, 1961).

70 The fractionation factor at equilibrium, $\alpha_{H_2O-H_2(eq)}$, is highly sensitive to temperature (e.g.,
71 Friedman and O'Neil, 1977; Richet et al., 1977), and is therefore useful as a geothermometer, which saw
72 early application to geothermal and fumarolic gases (Arnason, 1977; Friedman, 1953; Kiyosu, 1983;
73 Lyon and Hulston, 1984; Mizutani, 1983), and also fault gases (Kita et al., 1980). Geothermometers based
74 on fluid/gas chemistry are usually applied to solutions advected to the surface with the expectation that
75 they provide information about subsurface processes that cannot be directly observed or sampled in-situ.
76 This type of geothermometer therefore requires the elements or species involved to exhibit chemical or
77 isotopic disequilibrium relative to the conditions measured at the surface, where the solution sample was
78 acquired. For example, Fig. 1 plots the *measured* H_2 - H_2O fractionation factors (defined herein as α_{OBS})
79 against T measured at the point of sampling for a variety of geologic settings, and the field samples
80 commonly have α_{OBS} values that deviate from the equilibrium curve in a manner that indicates the
81 solution had previously experienced a higher T . This combined dataset also allows us to conclude that the
82 kinetics of D-H exchange between H_2 and H_2O is rapid for $T > \sim 300$ °C. Therefore, beyond a minimum
83 (apparent) T of formation, the amount of information to be gained from observed disequilibrium relies
84 foremost on understanding the relevant reaction kinetics.

85 Surprisingly, few constraints exist on uncatalyzed rates of H_2 - H_2O isotope exchange, especially
86 for H_2 dissolved in liquid water. Using an experimental apparatus that eliminates the need to account for
87 gas-liquid (multiphase) exchange, we have therefore derived the D-H exchange rate for dissolved H_2 at
88 three temperatures below 100 °C. These data may be used to help deduce residence or transit times for
89 fluid movement in the crust, and they also provide an important basis for identifying and quantifying the
90 extent to which microbial biomes catalyze D-H exchange with water. Furthermore, we use previously
91 published data on gas-phase exchange rates (Lecluse and Robert, 1994) to infer a solution density
92 dependence in the rate law. This formulation should serve to simplify the inclusion of H_2 - H_2O isotope
93 exchange kinetics in more complicated multiphase models that explore processes ranging from boiling in
94 geothermal systems (Drummond and Ohmoto, 1985; Spycher and Reed, 1988; Truesdell et al., 1977) to
95 the origin of water on Earth and elsewhere in the solar system (Albertsson et al., 2014; Genda and Ikoma,
96 2008; Lecluse and Robert, 1994; Niemann et al., 2010; Robert et al., 2000). Should better isotopic data
97 be obtained by future space missions, the new rate relationships may also prove valuable in assessing the
98 temperature of suspected subsurface oceans on icy satellites such as Enceladus, where H_2 has been

99 measured in plumes of vapor and particulates jetting from cracks in the frozen outer shell (Hsu et al.,
100 2015; Waite et al., 2017; Waite et al., 2009).

101

102 **2. METHODS**

103

104 **2.1. Experimental design and protocol**

105

106 The primary goal of this laboratory study was to observe the rate at which dissolved H₂
107 approaches isotopic equilibrium with H₂O at different temperatures. Starting reactants were grade 5
108 hydrogen gas, additionally filtered through a combined oxygen-moisture-hydrocarbon trap ($\delta D_{H_2} = -107$
109 ‰ VSMOW), and deuterium-enriched H₂O ($\delta D_{H_2O} \approx +5220$ ‰ VSMOW). The H₂ and H₂O were
110 therefore initially far from isotopic equilibrium for any T of interest. The most important factor for the
111 experimental design is that the dissolved H₂ remain undersaturated, and no gas phase (headspace) be
112 allowed to exist or develop as a result of sample acquisition. The experiment was therefore carried out in
113 a flexible gold reaction cell system, which is designed to monitor the time series progression of
114 hydrothermal reactions at constant pressure (P) and T (Berndt et al., 1996b; Seyfried et al., 1979; Seyfried
115 et al., 1987). Given all wetted parts consist of gold and titanium, this reactor is also the best option for
116 avoiding effects of both surface catalysis and H₂ diffusion over the course of the experiment (Lemke et
117 al., 2009; Palmer and Drummond, 1986; Reeves et al., 2012; Seward and Kishima, 1987).

118 This system consists of a flexible gold cell (~250 ml volume) with a passivated (oxidized)
119 titanium head (closure) and sampling tube that is sealed within a steel pressure vessel (Fig. 2). This entire
120 assembly is insulated within a rocking furnace, where desired temperature is maintained by proportional
121 control microprocessors. The Ti sampling tube terminates external to the steel vessel/furnace, and is
122 capped with a high-pressure Ti valve for extracting experimental solutions isolated in the gold cell. In
123 order to control system pressure, the void space within the steel vessel (external to the gold cell) is filled
124 with distilled water, and open to a valved network of tubing that includes in-line strain gauge transducers
125 and a high-pressure syringe pump. Because the gold reaction cell is flexible, the confining pressure in the
126 steel vessel and that within the reaction cell are equivalent. The system therefore permits isobaric
127 sampling by directing the syringe pump to maintain the desired confining pressure, while an aliquot of
128 reactant fluid is expressed by (carefully) opening the Ti valve. Essentially, an equal volume of confining
129 fluid is simultaneously added as sample fluid is being removed, and with each sample extracted (over the
130 course of the experiment), the gold cell incrementally collapses, much like a tube of toothpaste. New fluid
131 or gaseous reactants may similarly be introduced into the gold cell at any time (through the Ti valve) as
132 long as the maximum capacity is not exceeded.

133 The experimental setup was as follows. The gold cell was filled near capacity with the spiked
134 H₂O and sparged with grade 5 Ar gas for 45 mins to best eliminate other dissolved gases. The sparging
135 tube was removed, and the flow of Ar was then routed through the titanium closure assembly (includes
136 the valve and sampling tube and closure), which was loosely fitted into the gold cell. Prior to fully sealing
137 the Ti closure, any remaining headspace in the cell was allowed to purge for another 15 min. The Au-Ti
138 assembly was then sealed into the steel vessel with a full complement of confining water, and the system
139 was situated in the rocking furnace with a vertical orientation (i.e. the sampling tube pathway was
140 vertical, same as the orientation shown in Fig. 2). Still at ambient *P-T*, a syringe was attached to the Ti
141 sampling valve, the valve was opened, and additional confining water was pumped into the steel vessel
142 until reactant water began to appear in the syringe. This signified that the majority of the remaining Ar
143 headspace in the gold cell had been removed through the sampling tube. With the sampling valve then
144 closed, the system was pressure tested at 500 bars over night, and no leaks were detected. Pressure was
145 relieved to ambient, and a sufficiently large sample of reactant water was removed from the gold cell to
146 make room for a charge of H₂ gas (~20 ml). Prior to adding the H₂, the system was stabilized at the initial
147 experimental *T* of 97 °C in order to avoid ambiguous reaction progress during heating. With the apparatus
148 still oriented vertically (cf. Fig. 2), the gas line from the H₂ tank was flushed prior to sealing in the
149 (closed) Ti sampling valve, and was then pressurized to ~65 psig. Cell confining *P* was again balanced to
150 ambient, the Ti valve then opened, and the system registered the tank pressure. The piston in the syringe
151 pump was directed to retract at a constant rate, which allowed the tank pressure to expand the gold cell
152 with a (headspace) volume of H₂ roughly equivalent to the water volume received in the pump. Sufficient
153 H₂ was added to yield an estimated concentration of 10–20 mmolal, which is on the high end of values
154 measured in deep sea hydrothermal fluids (Charlou et al., 2002; Gallant and Von Damm, 2006;
155 McDermott et al., 2015; Schmidt et al., 2007; Seyfried et al., 2011; Seyfried et al., 2015). With the gold
156 cell then effectively charged (Ti valve now closed), the furnace was inverted (the sampling tube/valve
157 now facing the floor) in order to distance the H₂ bubble(s) from the sampling assembly before raising the
158 system pressure. This minimizes the amount of gas that might be compressed in and around the sampling
159 line, which would otherwise hinder the rate of dissolution, and also mitigates the risk of the first fluid
160 sample being inhomogeneous. The system was pressurized to 200 bars to speed H₂ dissolution, and the
161 first sample was acquired after 4.5 hrs. Thereafter the *P* was lowered and maintained at 70 bars for all *T*
162 conditions, which is (arbitrarily) ~3x higher than saturation for a solution of 20 mmolal H₂. Due to the
163 relatively large *T* dependence of D/H fractionation between H₂ and H₂O (Fig. 1), we were able to retrieve
164 rate constants for multiple temperatures (97, 54 and 22 °C) within a single experiment (see below).
165 Temperatures reported herein refer to a steel-sheathed type K thermocouple (chromel-alumel) in direct
166 contact with the confining fluid surrounding the gold cell. The temperature gradient in the system was

167 assessed by rocking the (tubular) furnace from horizontal through vertical orientations, which
168 redistributes heat flow relative to the static (horizontal) position maintained over the duration of the
169 experiment. During this process, T varied by less than 2 °C, which is comparable to the uncertainty of the
170 thermocouple. For the final leg of the experiment, the furnace T controls were shut off, and the system
171 cooled to that of ambient in the laboratory. The laboratory is climate controlled year round, and the
172 system read between 21 and 23 °C for the duration.

173 Gas-tight samples were acquired over the course of the experiment for quantitative analysis of
174 dissolved H_2 and δD_{H_2} . Samples for dissolved H_2 were taken into plastic syringes with a PTFE stopcock
175 for immediate analysis by gas chromatography. This measurement was performed periodically to assure
176 the H_2 concentration in the gold cell was not changing with time. A steady-state concentration of 18
177 mmolal was observed. Samples for δD_{H_2} were expressed directly from the reaction cell into sterile 60 ml
178 pyrex vials, sealed with crimped butyl rubber stoppers. The sampling assembly and procedure was as
179 follows. Two fine-gauged luer-lock needles were inserted through the stopper of the pyrex vial. Needle
180 (1) was connected to the Ti sampling valve using a 3-way PTFE stopcock (one extra "bleed" port was
181 available). Needle (2) was connected to a tank of grade 6 He gas. In this way, both the vial and sampling
182 assembly were thoroughly purged with He: in through needle (2) and out the bleed port of the stopcock,
183 which had a length of tubing that terminated under water to observe bubbling and prevent back flush.
184 With He still flowing, needle (2) was removed from the vial, and when bubbling ceased, communication
185 from the stopcock to the vial was closed. An empty syringe was placed in the bleed port, and the Ti
186 sampling valve was carefully opened until the syringe plunger slowly began moving. Once 1–2 mls of
187 water had accumulated in the syringe, communication was switched from the bleed port to the vial. The
188 bleed process served to discard the fluid fraction from the sampling line that was not at full experimental
189 T . Once 2–3 mls of water (plus exsolved H_2) had accumulated in the vial, the sampling valve was closed
190 and the vial stored for later analysis (see below). We note this sampling process naturally imparted a
191 slight over-pressure in the vial, which allowed us to easily acquire multiple subsamples of the gas
192 headspace.

193

194 **2.2. Analytical methods for the D/H (isotope) ratios of H_2 and H_2O**

195

196 The isotopic composition of H_2 was analyzed at the Center for Isotope Geochemistry (Lawrence
197 Berkeley National Laboratory) using a Thermo Scientific GC Trace Gas Ultra system connected to a
198 Thermo Scientific Delta V Plus Mass Spectrometer (IRMS). A volumetrically calibrated sample loop
199 attached to a 6-port valve system was flushed with sample gas, and the gas then injected onto the GC
200 column. H_2 was separated on an HP-molesieve fused silica capillary column (30 m x 0.320 mm) prior to

201 passing into the IRMS. Reproducibility of these analyses is ± 5 ‰ (2σ), as determined by repeated
202 analyses of 3 calibrated gas standards ($\delta D_{H_2(VSMOW)} = -762, -364$ and -124 ‰). Linearity of the IRMS is
203 also observed within the uncertainty noted above. Although the δD_{H_2} values measured in our experiments
204 fall outside the range calibrated on our instrument, there is little reason to expect this is problematic
205 because they amount to a modest ($< 2.5x$) increase in the D/H ratio relative to natural abundance.
206 Furthermore, previous studies have demonstrated excellent linearity for δD_{H_2} by IRMS over several
207 orders of magnitude (e.g., Hilkert et al., 1999; Morrison et al., 2001; Tobias et al., 1995). Experimental
208 samples were also re-analyzed at various (later) time intervals over the course of the study to make sure
209 there was no significant change in δD_{H_2} values during storage (at ambient T) between sampling and
210 analysis. The replicate analytical results differ by no more than 16 ‰ (average 8 ‰), indicating that once
211 the H_2 was degassed and diluted in the sample vial, the isotopic composition was effectively stable over
212 storage times employed (Table 1).

213 A deuterium-enriched water was used in the experiment to ensure the system was initially far
214 from isotopic equilibrium, and to facilitate large changes in δD_{H_2} that could be well resolved analytically
215 with reaction progress. The starting water was a mixture of 0.51 g of 99.9 % D_2O and 554.92 g of de-
216 ionized water ($\delta D_{H_2O} = +86$ ‰), which produced water with a δD_{H_2O} of $\sim +5200$ ‰. Despite the large
217 shifts in δD_{H_2} in the experiments, the mass balance of water in the system was sufficiently high that
218 concomitant changes in δD_{H_2O} were calculated to be negligible (< 0.5 ‰). The actual δD of the water
219 was analyzed using a Los Gatos Research liquid water analyzer (LGR). This required serially diluting the
220 solution with additional de-ionized water to within the calibrated linear range of the LGR ($\leq +836$ ‰).
221 Within uncertainty, no difference in δD_{H_2O} was observed between the unreacted starting water and water
222 recovered from the Au experimental cell upon conclusion of the experiment. Based on these
223 measurements, we calculated a δD_{H_2O} value of $+5220 \pm 50$ ‰ (2σ) for the experimental water. This
224 uncertainty is not critical when determining the kinetic rate constants from our experiments because these
225 are based only on relative changes in δD_{H_2} (see section 3.1). However, this does introduce a relatively
226 large error in calculations of the equilibrium isotope fractionation factors ($\alpha_{H_2O-H_2(eq)}$) at the 3 temperatures
227 used for these experiments (see section 4.2).

228 3. RESULTS

229
230 The raw experimental data are shown in Table 1 and Fig. 3. At the three temperatures studied,
231 near equilibrium conditions were ultimately achieved, indicated by an approach to steady-state δD_{H_2} with
232 time (Fig. 3). Observing the time series changes in δD_{H_2} , isotopic equilibrium was reached on timescales
233 of ~ 250 hrs at 97 °C, $\sim 1,500$ hrs at 54 °C, and $>12,000$ hrs at 22 °C. This corresponds to approximate half

234 lives for isotope exchange of about 2 days, 2 weeks, and 3 months at 97, 54 and 22 °C, respectively. The
 235 data also demonstrate that D–H isotope exchange between H₂O and H₂ is reversible. As discussed in more
 236 detail below, deriving appropriate rate constants for such reversible reactions requires defining the
 237 equilibrium value (e.g., Lasaga, 1998). In many instances, chemical reactions subject to kinetic studies do
 238 not equilibrate on laboratory timescales, which necessitates constraining expected equilibrium using
 239 empirical or theoretical relationships. For example, Fig. 3 compares our experimental results with
 240 equilibrium values of δD_{H_2} (or $\delta D_{H_2(eq)}$) calculated using the measured δD_{H_2O} ($\approx \delta D_{H_2O(eq)}$, +5220 ‰) and
 241 equations for $\alpha_{H_2O-H_2(eq)}$ after both Bardo and Wolfsberg (1976) and Horibe and Craig (1995). Despite
 242 general agreement, neither of these relationships best reflect the approach to equilibrium exhibited in the
 243 experiments at all three temperatures. Therefore, to extract accurate and internally consistent rate
 244 constants, values of $\delta D_{H_2(eq)}$ were extrapolated by fitting the experimental data from each T with an
 245 exponential function (Fig. 3), rather than depending on theoretically calculated values. Using these data,
 246 we describe in the following section the derivation of rate constants for D–H exchange between liquid
 247 H₂O and dissolved H₂ (or H_{2(aq)}).

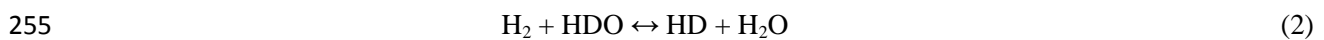
248

249 **3.1. Derivation of rate constants for D–H isotope exchange and their temperature dependence**

250

251 In our experimental system, D₂O and D_{2(aq)} species should be negligible because of the small
 252 abundance of D relative to H, so the reversible reaction under consideration may be represented as the
 253 exchange of one D between dissolved hydrogen and water:

254



256

257 Assuming first-order rate dependence for all species (e.g., Cole and Chakraborty, 2001) we can write the
 258 following differential equation in which reaction progress is traced by the change in the concentration of
 259 HD with time (t);

260

$$261 \quad d[HD] / dt = k'[H_2][HDO] - k[HD][H_2O] \quad (3)$$

262

263 and k' and k represent forward and reverse rate constants, respectively (Cole and Chakraborty, 2001;
 264 Criss, 1999; Criss et al., 1987). If the concentrations are expressed in units of moles per liter (mol/L), the
 265 k values have units of, for example, [L/mol] / hr. Isotopic equilibrium is attained when $d[HD]/dt = 0$, and
 266 this condition can therefore be described with the following expression:

267

268
$$k' / k = [\text{HD}_{(\text{eq})}][\text{H}_2\text{O}_{(\text{eq})}] / [\text{H}_{2(\text{eq})}][\text{HDO}_{(\text{eq})}] \quad (4)$$

269

270 where ratio k' / k is the equilibrium D/H fractionation factor (α_{eq}) for H_2 in equilibrium with H_2O . For
 271 reaction progress at any time between $t = 0$ and equilibrium, the mass balance in our experiment was
 272 designed such that changes in all species other than $[\text{HD}]$ were sufficiently negligible to allow the
 273 simplifying assumption that their concentrations remain equal to the starting values, which means they
 274 can also be represented as the equilibrium values. Therefore equation 3 may be written as;

275

276
$$d[\text{HD}_{(t)}] / dt = k'[\text{H}_{2(\text{eq})}][\text{HDO}_{(\text{eq})}] - k[\text{HD}_{(t)}][\text{H}_2\text{O}_{(\text{eq})}] \quad (5)$$

277

278 and subsequently integrated to yield:

279

280
$$[\text{HD}_{(t)}] = k'[\text{H}_{2(\text{eq})}][\text{HDO}_{(\text{eq})}] / k[\text{H}_2\text{O}_{(\text{eq})}] + C * \exp\{-k[\text{H}_2\text{O}_{(\text{eq})}]t\} \quad (6)$$

281

282 where C is the integration constant. The right side of equation 4 may be substituted for the k' / k term in
 283 equation 6, which simplifies to;

284

285
$$[\text{HD}_{(t)}] = [\text{HD}_{(\text{eq})}] + C * \exp\{-k[\text{H}_2\text{O}_{(\text{eq})}]t\} \quad (7)$$

286

287 At $t = 0$, $[\text{HD}_{(t)}] = [\text{HD}_{(i)}]$, the initial concentration of HD, and therefore $C = [\text{HD}_{(i)}] - [\text{HD}_{(\text{eq})}]$. Further
 288 defining $k[\text{H}_2\text{O}_{(\text{eq})}] = k_1$, the effective rate constant, we arrive at the expression:

289

290
$$([\text{HD}_{(t)}] - [\text{HD}_{(\text{eq})}]) / ([\text{HD}_{(i)}] - [\text{HD}_{(\text{eq})}]) = \exp\{-k_1 t\} \quad (8)$$

291

292 This represents a pseudo-first-order expression, and the left side of equation 8 equates to the fractional
 293 approach to equilibrium, often denoted as the quantity $1 - F$ (i.e. $F = 1$ at equilibrium), and may be
 294 equivalently cast in terms of isotope ratios (e.g., D/H) or delta (δ) values (Cole and Chakraborty, 2001;
 295 Criss, 1999; Criss et al., 1987). For convenience, we use the measured $\delta\text{D}_{\text{H}_2}$ values in the following
 296 expression to treat our experimental data:

297

298
$$\ln \{(\delta\text{D}_{\text{H}_2(t)} - \delta\text{D}_{\text{H}_2(\text{eq})}) / (\delta\text{D}_{\text{H}_2(i)} - \delta\text{D}_{\text{H}_2(\text{eq})})\} = -k_1 t \quad (9)$$

299

300 If the assumption of first-order behavior is appropriate, the left side of equation 9, plotted versus time,
 301 should be linear, with slope = $-k_1$, and intercept at the origin. Regressions of the isotopic data and the

302 derived rate constants (k_1) using equation 9 are shown in Fig. 4; and an associated Arrhenius plot displays
303 an excellent correlation with T , yielding an activation energy (E_a) of 52 kJ/mol (Fig. 5).

304

305 4. DISCUSSION

306

307 Previously published data that is directly comparable to our liquid-phase D–H exchange rates are
308 scarce. Lyon and Hulston (1984) note a half-life of ~10 mins at 225 °C, and Jeffrey and Kaplan (1988)
309 report a shift in δD_{H_2} from -195 to -672 ‰ ($\delta D_{H_2O} = -92$ ‰) after 4 months at ~25 °C. These observations,
310 although not fully documented in the papers, are nonetheless consistent with our results (Fig. 5). Our
311 experiment was conducted at sub-neutral pH (~5.6 at 22 °C), and we note several other laboratory studies
312 indicate the rate of isotope exchange with H_2 is catalyzed by high concentrations of hydroxide ion,
313 whereas increasing acidity seems to have little effect (Flournoy and Wilmarth, 1961; Miller and
314 Rittenberg, 1958; Wilmarth et al., 1953). The extent to which rates reported in these previous studies are
315 quantitatively comparable to ours is uncertain because data are typically not tabulated, and they were
316 mostly derived from systems where steam was coexisting with highly basic solutions ($\gg 0.1$ molal $[OH^-]$).
317 These other studies were concerned with the mechanism of hydroxide catalysis to the extent that a T -
318 independent "background rate" for reaction with solvent water was subtracted for solutions where $[OH^-] <$
319 1 molal (Flournoy and Wilmarth, 1961). While hydroxide catalysis appears considerable, the relative
320 effect within the range of $[OH^-]$ observed in natural solutions may be less significant. For example, in a
321 0.011 molal hydroxide solution at 65 °C, Symons and Buncl (1973) calculate a k_1 value 1.5x larger than
322 we observe (Fig. 5). This is a modest enhancement of the kinetics for a solution that amounts to a pH(25
323 °C) of ~12, which is on the high end of values reported from natural alkaline springs (e.g., Etiope et al.,
324 2017; Neal and Stanger, 1983; Suda et al., 2014). Considering the heterogeneity of natural aqueous
325 solutions, there is nonetheless potential for other dissolved components to affect rates of isotope
326 equilibration between H_2 and H_2O . In addition, microbial metabolism can significantly speed progress
327 towards equilibrium (Campbell et al., 2009; Kawagucci et al., 2011; Kawagucci et al., 2014; Okumura et
328 al., 2016; Romanek et al., 2003; Valentine et al., 2004; Vignais and Billoud, 2007).

329 Given currently available constraints, the expression for k_1 shown in Fig. 5 appears acceptable for
330 generally representing uncatalyzed rates of D–H exchange between $H_{2(aq)}$ and liquid H_2O . However, the
331 experiments of Lecluse and Robert (1994) suggest exchange rates (k_1) in the gas phase are slower by
332 several orders of magnitude. In the next section, we therefore compare our new results to the gas-phase
333 data of Lecluse and Robert (1994), with the aim of developing a universal rate expression that accounts
334 for how phase changes impact the isotope exchange kinetics. Isotope fractionation between gas/vapor
335 and liquid phases also plays a role in accounting for the variability in predicted equilibrium D/H

336 fractionation ($\alpha_{\text{H}_2\text{O}-\text{H}_2(\text{eq})}$), exemplified in Fig. 3. The implications of this are discussed in section 4.2,
337 where we use the best available data to derive updated representations for the temperature dependence of
338 $\alpha_{\text{H}_2\text{O}-\text{H}_2(\text{eq})}$. In subsequent sections (4.3–4.6) we use the new kinetic and equilibrium relationships obtained
339 in sections 4.1 and 4.2, respectively, to build kinetic models that can account for non-equilibrium D/H
340 fractionation where observed in natural geologic systems.

341

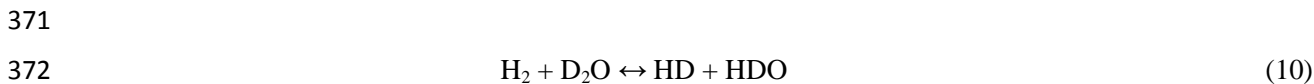
342 **4.1. A general expression for D–H exchange rates in both gaseous and liquid systems based on** 343 **phase density**

344

345 The simplicity of Equation 9 suggests it may be possible to extend rates of D/H equilibration in
346 liquid water to systems that are dominated by gas phases. To evaluate this we compare our experimental
347 results to those of Lecluse and Robert (1994), who derived rate data from individual batch reactions
348 between H_2 and D_2O gas, carried out in a glass tube apparatus. These gas phase reactions were performed
349 with and without the presence of potential natural catalysts, the objective being to understand isotopic
350 evolution in the solar nebula. They report the initial partial pressures of each gas at ambient T (total P
351 averaged ~ 0.08 atm), and the change in D/H ratio of the H_2 gas after reaction for a given time at
352 temperatures up to 400 °C.

353 Lecluse and Robert (1994) concluded that the catalysts they employed had no meaningful effect
354 on rates of D–H exchange, and treated all of their data together. However, due to what we perceive as
355 inconsistencies, we eliminate from consideration their results from experiments conducted with either
356 activated charcoal or montmorillonite (clay). For example, Lecluse and Robert (1994) note that rates
357 obtained from experiments with charcoal appear systematically faster, despite the difference being
358 statistically insignificant. In addition, many of the experiments conducted with charcoal and clay utilized
359 substrate the authors had pre-enriched with D_2O , and in several of these cases they report D_2O partial
360 pressures in excess of steam-saturation pressure at the applicable T , with the derivation of these values
361 being unclear. We also neglect data for $T < 100$ °C because the rates depicted graphically in Lecluse and
362 Robert (1994) are much lower than those that can be calculated using their tabulated data. More
363 specifically, the average rates calculated for 65 °C (2 experiments) and 25 °C (11 experiments) are both
364 higher than that at 100 °C (11 experiments), in which case the authors note (for an unspecified number of
365 experiments) that, "when no exchange was detected, rate constants are not reported in the tables but were
366 taken into account in the mean values plotted in [figures]". The remainder of the data we evaluate below
367 consist of 40 experiments conducted at temperatures between 100 and 400 °C.

368 One important difference between our experiments and those of Lecluse and Robert (1994) is that
 369 their starting reactant was D₂O, a species we assumed to be of negligible concentration in our
 370 experiments. The exchange reaction they investigated was therefore:



373
 374 and the reaction rate is then written as:

375
 376
$$d[\text{HD}_{(i)}] / dt = k'[\text{H}_2][\text{D}_2\text{O}] - k[\text{HD}][\text{HDO}] \quad (11)$$

377
 378 Lecluse and Robert (1994) ultimately derived an equation analogous to equation 9 to describe their
 379 experiments, expressed in the following form:

380
 381
$$\ln \left\{ \frac{(2[\text{D}/\text{H}]_{\text{H}_2(i)} - X_{\text{D}_2\text{O}})}{(2[\text{D}/\text{H}]_{\text{H}_2(i)} - X_{\text{D}_2\text{O}})} \right\} = -k_1 t \quad (12)$$

382
 383 where:

384
 385
$$X_{\text{D}_2\text{O}} = [\text{D}_2\text{O}_{(i)}] / ([\text{D}_2\text{O}_{(i)}] + [\text{H}_2(i)]) \quad (13)$$

386
 387 and

388
 389
$$k_1 = k'([\text{D}_2\text{O}_{(i)}] + [\text{H}_2(i)]) / \alpha_{\text{H}_2\text{O}-\text{H}_2(\text{eq})} \quad (14)$$

390
 391 Equations 12–14 were used to extract k_1 and k values using the raw data of Lecluse and Robert (1994),
 392 recognizing that $k' = k / \alpha_{\text{H}_2\text{O}-\text{H}_2(\text{eq})}$. Although these authors cast their rates in terms of gas partial pressures,
 393 we instead used concentration units of mol/L, because this simultaneously accounts for system density,
 394 and is ultimately more conducive to comparing rates observed in the gas phase with those in liquid H₂O.
 395 In this case the units of k are then [L/mol]/hr. Recalling our derivation of k_1 in condensed H₂O (section
 396 3.1, equations 7, 8), we defined k_1 (hr⁻¹) = $k[\text{H}_2\text{O}]$. We therefore calculated k values using the k_1 data
 397 given in Fig. 4 and the density of pure water at each T and P (~55 mol/L). The results show excellent
 398 agreement between our experiments and those of Lecluse and Robert (1994) for the T dependence of the
 399 rate constants k (Fig. 6a). A weighted regression of the combined datasets yields the following
 400 relationship;

401

402
$$\ln k = 9.186 - 6298 / T$$
 (15)

403

404 where k is in units of [L/mol]/ hr, and T is absolute temperature (K).

405 In general, for any H₂O + H₂ system, regardless of phase, we infer that the effective first-order
406 constant (k_1) that will describe the rate of approach to isotopic equilibrium is:

407

408
$$k_1 = k([H_2O] + [H_2])$$
 (16)

409

410 where [H₂O] and [H₂] are the concentrations of each species (including isotopologues) in mol/L, which
411 will be a function of T , P , and the full chemical composition of the system. Under many circumstances,
412 we may consider $k_1 \approx k[H_2O]$ to adequately represent the rate constant because H₂O is usually the
413 predominant component. This then yields a simplified full expression for k_1 ;

414

415
$$k_1 = [H_2O] 9764.61 * \exp\{-6298 / T\}$$
 (17)

416

417 where [H₂O] may be constrained as the density of water at the T and P of interest (ρ_w , in mol/L), and k_1
418 has units of hr⁻¹. The overall T dependence yields an E_a of 52.4 ± 1.3 kJ/mol (95% CI), which is
419 (expectedly) within the uncertainty of that derived in Fig. 5 because the lower uncertainty of our data
420 carried greater weight in the regression (Fig. 6a). However, an independent extrapolation of the k_1 values
421 derived from Lecluse and Robert (1994) gives a similar value of 48 ± 14 kJ/mol, which indicates the same
422 reaction mechanism in both condensed water and gas scenarios, suggesting the isotope exchange rate may
423 be largely a function of molecular collision frequency. The broader use of our simple density-based
424 relationships therefore seems reasonable until more data become available.

425 In order to provide an example of the predicted effect of density on the isotope exchange rate, we
426 use equation 17 to calculate and compare k_1 values along the vapor and liquid branches of the H₂O steam
427 saturation curve (Fig. 6b). For pure H₂O, at any given T along this curve (between 0 °C, the freezing
428 point, and 374 °C, the critical point), system pressure is fixed by the coexistence of liquid H₂O and
429 saturated H₂O vapor. Although the fugacity of H₂O in both the liquid and vapor are equivalent (at any
430 fixed T), the difference in the density of H₂O between the coexisting phases can be substantial. Figure 6b
431 implies that the effective k_1 in a closed (and isothermal) system, where saturated H₂O vapor exists, should
432 lie somewhere between the two end-member k_1 values calculated for the vapor and liquid phases,
433 depending roughly on the volume fraction of each phase. However, the natural occurrence of immiscible
434 phases in most geological settings is the result of open system conditions, where solutions experience

435 changes in temperature and/or pressure; and differences in the density of these phases, once developed,
436 also promotes their segregation.

437

438 **4.2. Updated representations for the temperature dependence of equilibrium isotope fractionation** 439 **in the H₂–H₂O system**

440

441 The equilibrium values of δD_{H_2} derived by extrapolation of curves fit to our experimental data
442 (Fig. 3) provide an independent comparison of our results with the predicted T -dependent equilibrium
443 fractionation between H₂O and H₂ ($\alpha_{H_2O-H_2(eq)}$). The new data compare favorably, falling between
444 representative curves for gaseous H₂ in equilibrium with H₂O liquid (denoted $\alpha_{H_2O(L)-H_2(g)}$) and H₂O vapor
445 (denoted $\alpha_{H_2O(v)-H_2(g)}$, Fig. 7), where the $\alpha_{H_2O(v)-H_2(g)}$ and $\alpha_{H_2O(L)-H_2(g)}$ curves differ by the vapor–liquid
446 fractionation factor of H₂O (Horibe and Craig, 1995; Horita and Wesolowski, 1994). The $\alpha_{H_2O(L)-H_2(g)}$
447 curve has previously been used to describe equilibrium for H₂ dissolved in liquid H₂O, but this would
448 only be correct if there were no isotope fractionation between gaseous and dissolved H₂ (or H_{2(g)}} and
449 H_{2(aq)}, respectively). However, Knox et al. (1992) report a H_{2(aq)}–H_{2(g)} isotope fractionation factor of 1.037
450 at 21 °C. When this is factored with the $\alpha_{H_2O(L)-H_2(g)}$ relationship, it results in a fractionation factor of 3.786
451 (grey triangle, 21 °C, Fig. 7), which is within the uncertainty of what we report for liquid H₂O and H_{2(aq)}.

452 The $\alpha_{H_2O(v)-H_2(g)}$ and $\alpha_{H_2O(L)-H_2(g)}$ curves in Fig. 7 ultimately converge with increasing T along the
453 vapor-liquid envelope of water. Beyond this region, experimental and theoretical calculations still largely
454 concern coexistence of H₂ with H₂O vapor, which may not best reflect isotopic fractionation in higher
455 density crustal fluids (Foustoukos and Mysen, 2012). Nonetheless, potential differences are likely to be
456 small, especially for purposes of geothermometry at high temperatures, where equilibrium α values
457 converge and approach unity (Criss, 1999). For example, the data of Fu et al. (2007) yield a reproducible
458 $\alpha_{H_2O-H_2}$ of 1.47 at 400 °C and 500 bars, which falls within the range of $\alpha_{H_2O-H_2(eq)}$ values predicted by
459 currently established ($\alpha_{H_2O(v)-H_2(g)}$) correlations (Bardo and Wolfsberg, 1976; Richet et al., 1977; Suess,
460 1949). Equilibrium isotope fractionation factors become more uncertain with decreasing T , considering
461 the exponential increase in $\alpha_{H_2O-H_2(eq)}$, and a paucity of experimental data for $T < 100$ °C (even in the
462 gaseous system).

463 Using the limited low- T data for $\alpha_{H_2O-H_2(eq)}$, including those herein, we have produced an
464 equilibrium curve for isotope fractionation between H₂O_(liq) and H_{2(aq)}, which we refer to as $\alpha_{H_2O(L)-H_2(AQ)}$
465 (Fig. 7, Supplementary Information). This was done by first regressing a new $\alpha_{H_2O(v)-H_2(g)}$ curve,
466 combining experimental and theoretical data where good agreement is observed (Bardo and Wolfsberg,
467 1976; Fu et al., 2007; Suess, 1949). Similar to Horibe and Craig (1995), we then derived a new
468 relationship for $\alpha_{H_2O(L)-H_2(g)}$ using the vapor–liquid (D/H) fractionation factors of H₂O given by Horita and

469 Wesolowski (1994). These $\alpha_{\text{H}_2\text{O}(\text{v})-\text{H}_2(\text{g})}$ and $\alpha_{\text{H}_2\text{O}(\text{L})-\text{H}_2(\text{g})}$ curves provided a basis for establishing a
470 reasonable and internally consistent representation of $\alpha_{\text{H}_2\text{O}(\text{L})-\text{H}_2(\text{AQ})}$. The $\alpha_{\text{H}_2\text{O}(\text{v})-\text{H}_2(\text{g})}$ and $\alpha_{\text{H}_2\text{O}(\text{L})-\text{H}_2(\text{g})}$ curves
471 coincide for $T > \sim 220$ °C, and the data of Fu et al. (2007), obtained at supercritical T and P , support the
472 assumption that $\alpha_{\text{H}_2\text{O}(\text{L})-\text{H}_2(\text{AQ})} = \alpha_{\text{H}_2\text{O}(\text{v})-\text{H}_2(\text{g})}$ at these conditions. The new $\alpha_{\text{H}_2\text{O}(\text{L})-\text{H}_2(\text{AQ})}$ regression therefore
473 included calculated values of $\alpha_{\text{H}_2\text{O}(\text{v})-\text{H}_2(\text{g})}$ for this (higher) T range. Data constraining the lower T range of
474 the regression are shown in Fig. 7, which, in addition to our results, includes values calculated using
475 $\alpha_{\text{H}_2\text{O}(\text{L})-\text{H}_2(\text{g})}$ and previously published $\text{H}_2(\text{aq})-\text{H}_2(\text{g})$ isotope fractionation factors, as exemplified by the Knox
476 et al. (1992) datum noted above (see Supplementary Information for further details). Table 2 provides
477 new polynomial coefficients for calculating $\alpha_{\text{H}_2\text{O}-\text{H}_2(\text{eq})}$ in the $\text{H}_2-\text{H}_2\text{O}$ system. These relationships indicate
478 $\alpha_{\text{H}_2\text{O}(\text{v})-\text{H}_2(\text{g})} \approx \alpha_{\text{H}_2\text{O}(\text{L})-\text{H}_2(\text{AQ})}$ for $T > 110$ °C, and the 95% prediction limits are $\alpha_{\text{H}_2\text{O}(\text{v})-\text{H}_2(\text{g})} \pm 0.018$ and
479 $\alpha_{\text{H}_2\text{O}(\text{L})-\text{H}_2(\text{AQ})} \pm 0.025$, although these uncertainties increase for $T < 15$ °C (see Fig. S4).

480 When comparing field data (α_{OBS}) to equilibrium fractionation there is generally some uncertainty
481 about which $\alpha_{\text{H}_2\text{O}-\text{H}_2(\text{eq})}$ applies (Fig. 7), because it will depend on the nature of the sample and how it was
482 acquired. In open (natural) systems, the low aqueous solubility of H_2 may result in exsolution prior to or
483 during sampling such that whether to reference $\alpha_{\text{H}_2\text{O}(\text{L})-\text{H}_2(\text{AQ})}$ or $\alpha_{\text{H}_2\text{O}(\text{L})-\text{H}_2(\text{g})}$ requires considering mass
484 balance. For example, if kinetic isotope effects are minimal, it might be reasonable to expect that $\delta\text{D}_{\text{H}_2}$
485 measured in free gas that has exsolved from continental spring waters should be referenced to $\alpha_{\text{H}_2\text{O}(\text{L})-\text{H}_2(\text{g})}$
486 ($\text{H}_2\text{O}(\text{liq})-\text{H}_2(\text{g})$, given $\delta\text{D}_{\text{H}_2\text{O}}$ is usually measured in the liquid). This assumes vapor–liquid isotopic
487 equilibrium was achieved during degassing, whether or not the previously dissolved H_2 was in
488 equilibrium with the H_2O . However, this assumption is generally unnecessary because gas/liquid
489 distribution coefficients (K_d) for H_2 exceed $7 \cdot 10^4$ for $T < 100$ °C (Fernandez-Prini et al., 2003), making it
490 difficult to shift the $\delta\text{D}_{\text{H}_2}$ of exsolved gas relative to the $\delta\text{D}_{\text{H}_2}$ of the bulk system unless D–H exchange
491 with H_2O in the gas (or vapor) can occur. Sufficient exchange is unlikely due to the sluggish kinetics in a
492 gas/vapor phase even at 100 °C (e.g., $1/k_1 \approx 7$ yrs vs. ~ 2 days in the liquid, Fig. 6b). Therefore $\alpha_{\text{H}_2\text{O}(\text{L})-\text{H}_2(\text{AQ})}$
493 ($\text{H}_2\text{O}(\text{liq})-\text{H}_2(\text{aq})$) is usually the best equilibrium reference whenever the sampled water phase is a
494 liquid. Ultimately, the apparent T of samples calculated using $\alpha_{\text{H}_2\text{O}(\text{L})-\text{H}_2(\text{AQ})}$ are as much as ~ 8 °C lower
495 than those derived using $\alpha_{\text{H}_2\text{O}(\text{L})-\text{H}_2(\text{g})}$, which is a modest uncertainty. However, the distinction has greater
496 impact on results of kinetic models, especially at lower T , because time to equilibration is proportional to
497 the degree of isotopic disequilibrium (equation 9).

498 499 **4.3. Application of kinetic models to D/H isotope fractionation observed in natural geologic systems** 500

501 When T at the point of sampling is known, our kinetic data allows us to use the δD values of H_2
502 and H_2O measured in natural fluids (Fig. 1) to infer aspects of hydrology such as fluid transit times in the

503 crust and their average flow velocity, depending on the availability of additional constraints. Here we
504 focus mostly on interpreting data from hydrothermal and volcanic systems. We develop simple kinetic
505 models of D–H exchange that simulate effects of cooling as fluids/gases flow up through the crust; away
506 from a high- T (magmatic) heat source, where H_2 and H_2O are likely to be in isotopic equilibrium, and
507 towards the surface, where samples are obtained. The models use the first-order rate equation (9), and the
508 T - ρ_w -dependent expression for k_1 (equation 17) to calculate how δD_{H_2} evolves as a function of a specified
509 cooling rate and the initial T of H_2 – H_2O isotopic equilibrium. For example, the kinetic fractionation trends
510 shown in Figs. 8–10 (see sections 4.4–4.5 below) were derived by calculating the change in δD_{H_2} with
511 incremental (step-wise) decreases in T of 0.5 °C, where k_1 is a function of T and an assumed P (i.e. T and
512 P yield density), and t (hrs) across each step is a function of the imposed conductive cooling rate (°C / hr).
513 For the geologic scenarios subsequently considered, finer scale step sizes in T did not noticeably improve
514 the resolution of the model curves.

515 Simplifying assumptions in the models are that mineral surfaces are non-catalytic and that no new
516 H_2 is generated during cooling. The latter assumption is reasonable because H_2 fugacity decreases with T
517 for (mineral) redox buffers applicable to natural hydrothermal systems (e.g., McDermott et al., 2018;
518 Shock, 1992; Sleep et al., 2004), and H_2 generation due to mineral precipitation should be negligible
519 (Seewald and Seyfried, 1990; Seyfried and Ding, 1995). Microbial enhancement of δD_{H_2} equilibration
520 rates is well documented, even under scenarios of H_2 consumption, and is considered where fluids have
521 cooled below ~100 °C (Campbell et al., 2009; Kawagucci et al., 2011; Kawagucci et al., 2014; Vignais
522 and Billoud, 2007). Multi-phase behavior is also a complicating factor, although the density dependence
523 of our rate expression makes accounting for this tractable. The density issue is mitigated when
524 considering deep-sea hot springs (section 4.4) because the overburden of seawater usually exceeds sub-
525 critical vapor pressures during hydrothermal circulation (Bischoff, 1991; Bischoff and Rosenbauer, 1985),
526 and extensive boiling or gas exsolution is uncommon save during eruptions and magmatic events
527 (Butterfield et al., 2011; Konno et al., 2006; Lilley et al., 2003; Lupton et al., 2006; Pester et al., 2014;
528 Seewald et al., 2003; Von Damm, 2000). The density effect on k_1 in submarine settings is therefore
529 minimal compared to continental settings where a low-density steam or gas phase can more easily
530 develop (Fig. 6b). In the latter cases we assume there is no kinetic isotope separation associated with
531 boiling and phase segregation, which might otherwise affect the residual δD_{H_2} measured in geothermal
532 liquids/vapors.

533

534 **4.4. Deep-sea hydrothermal systems**

535

536 **4.4.1. Black smoker vents**

537

538 Deep sea hydrothermal activity is ubiquitous along mid-ocean ridge and back-arc spreading
539 systems, where seawater circulates close to active magma bodies and reacts with rock at elevated
540 temperatures and pressures (e.g., Baker and German, 2004; Edmond et al., 1979; German and Seyfried,
541 2014; Kelley et al., 2002; Reeves et al., 2011). Hydrothermal fluids exit the seafloor at temperatures up to
542 ~400 °C, and the hottest of these vents are known as "black smokers", referring to the rapid precipitation
543 of transition metals upon mixing with cold seawater (Haymon, 1983; Tivey et al., 1990). The chemical
544 composition of these fluids, including the H₂ concentration, is a function of T and the lithology of the
545 reacting substrate (Seyfried et al., 1991; Seyfried et al., 2010; Seyfried et al., 2015). Previous
546 investigations have demonstrated that α_{OBS} in black smokers appear to be in isotopic equilibrium at T
547 measured during sampling on the seafloor (Horibe and Craig, 1995; Kawagucci et al., 2011; Kawagucci et
548 al., 2010; Proskurowski et al., 2006). The Fe and Mn concentrations, however, indicate fluid–mineral
549 equilibration at higher T , between 400 and 450 °C, which translates to a (roughly) estimated conductive
550 cooling rate of 50 °C / hr (Pester et al., 2014; Pester et al., 2011; Wilcock, 2004). We used this cooling
551 rate to derive a kinetic fractionation trend which assumed initial isotopic equilibrium at 450 °C, and k_1
552 values at each temperature step were calculated using a near-critical density of 33 mol/L for $T > 373$ °C,
553 transitioning to densities along a 220 bar isopleth for lower temperatures. This approach is consistent with
554 the typical hydrostatic load at 1500 to 3000 m below sea level, and broadly applicable to most deep sea
555 hydrothermal systems. The resulting model curve is consistent with field data from black smokers, which
556 both indicate the exchange kinetics are fast enough to maintain isotopic equilibrium as end-member fluids
557 cool during ascent to the seafloor for $T > \sim 250$ °C (Fig. 8a).

558 Fluids exiting the seafloor at lower T predominantly reflect subseafloor mixing between seawater
559 and pure hydrothermal fluid (Edmond et al., 1979; Pester et al., 2008; Von Damm and Lilley, 2004), and
560 the extent of mixing is given by the dissolved Mg concentration, which is effectively zero in the
561 hydrothermal end-member (Seyfried, 1987; Von Damm et al., 1985). Unique datasets presented by
562 Kawagucci et al. (2010, 2011), which report both Mg and $\delta\text{D}_{\text{H}_2}$ values, demonstrate how such mixing
563 effectively quenches the high- T isotopic signature of the hydrothermal fluid (Fig. 8). However, we note
564 data acquired near the Monju structure of the Kairei vent field (Central-Indian Ridge), and NBC vent in
565 the Iheya North vent field (mid-Okinawa Trough) because these are the only data reported where both
566 low- and high- T fluids were sampled in sufficiently close proximity to possibly share a similar
567 hydrothermal end-member. In both cases, H_{2(aq)} in fluids diffusing from the seafloor surrounding the
568 respective black smokers exhibits lower $\delta\text{D}_{\text{H}_2}$ with decreasing T . This observation would be expected for
569 fluids approaching equilibrium, but the magnitude of the isotopic shifts is too large to be consistent with
570 the kinetic data at such (low) temperatures. We could find few reasonable combinations of mixing and

571 cooling to explain these observations unless the low- T (mostly seawater) end-member already contained a
572 fraction of $H_{2(aq)}$ in isotopic equilibrium at near ambient conditions (on the order of ~2% of the
573 concentration in the end-member vent fluid). Such a scenario might be consistent with near-equilibrium
574 α_{OBS} values measured in pore fluids of deep-sea sediments (Toki et al., 2011). Regardless of the presence
575 or absence of sediments in near-seafloor flow pathways, these observations from Monju and NBC vent
576 indicate that micro-organisms are likely catalyzing D–H exchange and enhancing the rate of isotopic
577 equilibration. Chemosynthetic microbes are ubiquitous in hydrothermal systems, taking advantage of
578 reduced metals and volatiles for metabolic energy once fluids are mixed to sufficiently low T (e.g.,
579 Jannasch and Mottl, 1985; Orcutt et al., 2011; Reysenbach et al., 2006). The data from Monju vent
580 suggest microbial catalysis becomes effective at $T \leq \sim 60$ °C (Fig. 8).

581 The biologically enhanced equilibration rate we calculate after Kawagucci et al. (2011) (see Fig.
582 5) is facilitated by the fact that these researchers collected three gas-tight samples of the same low- T
583 effluent from NBC vent, but they incubated two of the samples for later shipboard processing (remained
584 pressurized, and H_2 dissolved at 25 °C). After 48 hrs they observed the δD_{H_2} had shifted from -635 ‰
585 (datum shown in Fig. 8) to -736 ‰ (near equilibrium). These data therefore indicate this naturally
586 occurring microbial assemblage accelerated the D–H exchange of H_2 with water by a factor of ~600x
587 relative to the abiotic rate established in our experiments.

588

589 ***4.4.2. The Lost City hydrothermal system***

590

591 When compared to the hot/acidic black smokers that typically characterize mid-ocean ridges,
592 hydrothermal effluent of the Lost City vent field reflects different physical and chemical controls
593 (Blackman et al., 2002; Blackman et al., 2014; Boschi et al., 2006; Kelley et al., 2001; Kelley et al., 2005;
594 Titarenko and McCaig, 2016). At Lost City, H_2 -rich fluids with high pH (up to 10.7 at 25 °C) are
595 diffusing out of carbonate-brucite chimneys built upon a fault structure of the Atlantis Massif. Maximum
596 exit temperatures measured during sampling approach 100 °C, and the fluid chemistry indicates deep-
597 seated fluid–mineral reactions at temperatures up to ~250 °C, including a significant contribution from
598 the serpentinization of ultramafic rock (Allen and Seyfried, 2004; Foustoukos et al., 2008; Kelley et al.,
599 2005; Seyfried et al., 2015). Similar to the geochemical controls on black smoker fluid chemistry, these
600 reactions result in the removal of seawater Mg. Despite the lower temperature of the fluids venting at Lost
601 City, they still contain low dissolved Mg (Lang et al., 2012; Seyfried et al., 2015), indicating the
602 measured temperatures are primarily the result of conductive cooling rather than subseafloor mixing with
603 seawater (cf. Fig. 8).

604 Hydrogen isotope data from Lost City (Proskurowski et al., 2006) indicate the fluids fall into two
605 groups: 1) those venting at higher T , which have the highest H_2 concentrations and δD_{H_2} values, and 2)
606 those venting at (slightly) lower T with lower H_2 concentrations and δD_{H_2} values (Fig. 9). The highest T
607 samples, from Beehive vent (91 °C), best represent the (unmixed) hydrothermal end-member of the group
608 1 fluids (Lang et al., 2012; Proskurowski et al., 2006; Seyfried et al., 2015), and the δD_{H_2} values are
609 unlikely to be influenced by microbial activity. We therefore fit cooling models to the measured Beehive
610 T and the range of α_{OBS} measured in the group 1 fluids using constraints similar to those applied to black
611 smoker vents in the previous section. In this case we assumed initial H_2 – H_2O isotopic equilibrium at 250
612 °C, and the best fit to the group 1 data gives a conductive cooling rate of 0.31 to 0.44 °C / hr. The
613 chemistry of the fluids indicates the last T of fluid–mineral equilibration is ~190 °C (Seyfried et al.,
614 2015), and, using this as a benchmark, the cooling rate translates to a residence time of ~11 days in the
615 upflow zone at Lost City.

616 Independent information regarding heat flow and fluid circulation in the Atlantis Massif may be
617 estimated using data from Hole D of IODP Site U1309. Although it is unclear if these observations are
618 analogous to the seafloor structure directly below Lost City (Blackman et al., 2014; Titarenko and
619 McCaig, 2016), extending the thermal gradient measured in U1309D to 190 °C gives a depth of ~1.75 km
620 below seafloor, which suggests fluids are approaching the seafloor at ~7 m / hr. While this rate has
621 considerable uncertainty, it could be used as a constraint in testing multi-dimensional heat/fluid flow
622 models (e.g., Kim et al., 2015; Wanner et al., 2014).

623 The group 2 fluids (Fig. 9) discharge at lower temperatures in geographic locations more distal
624 (~50–100 m) to the center of the vent field. This indicates additional conductive cooling occurs in more
625 horizontal flow pathways near the seafloor or within the carbonate structures (Lang et al., 2012;
626 Proskurowski et al., 2006). However, kinetic models fit to the δD_{H_2} data of group 2 would require a
627 cooling rate ~5x slower than for group 1, which would imply the group 2 fluids have a substantially
628 different (e.g., more tortuous) upflow pathway. This seems unlikely given both the spatial scale of the
629 vent field, and the modest difference in exit temperatures between the two groups. Another explanation is
630 that group 2 fluids have a longer residence time in flow pathways near the seafloor such that they have
631 cooled to temperatures where microbes begin to thrive and catalyze isotope equilibration. The data of
632 Lang et al. (2012) provide further evidence to support this scenario. These data demonstrate that the group
633 2 fluids are depleted in both H_2 and sulfate, and enriched in bisulfide, relative to the group 1 fluids, which
634 is consistent with microbial sulfate reduction. Therefore, similar to the mixed fluids of Monju vent (Fig.
635 8), the Lost City data also suggest that microbial catalysis of H_2 – H_2O isotope exchange becomes an
636 important consideration at $T < \sim 60$ °C (Fig. 9).

637

638 4.5. Continental volcanic and geothermal systems

639

640 The highest temperature field observation for which α_{OBS} is reported comes from degassing
641 magma in the Surtsey Volcano of Iceland (Arnason and Sigurgeirsson, 1968), and these values are indeed
642 consistent with equilibrium at the measured crater T of ~ 1150 °C (Fig. 10). Other steam and gas
643 dominated fumaroles vent from volcanic terrains at temperatures that extend down to ~ 100 °C (i.e.
644 boiling at ~ 1 atm). This broad T range reflects variability in the distance and crustal permeability
645 separating the magmatic heat source and the surface, with the Surtsey magma being an extreme example.
646 Surface exhalations may result from any combination of vapor or liquid dominated flow pathways,
647 depending on geologic and hydrologic controls (Fournier, 1989; Harvey et al., 2015; Lowenstern et al.,
648 2012; Scott et al., 2015; Scott et al., 2014; Truesdell et al., 1977; White et al., 1971). Consequently,
649 relative to the deep-sea systems discussed above, D–H exchange rates in continental systems have more
650 variability, and modeling the cooling history of these fluids has more uncertainty.

651 To evaluate the magnitude of density effects on k_1 (equation 17) we use a cooling rate of $1^\circ\text{C} / \text{hr}$
652 in three kinetic models where the ρ_w associated with each T is in one case constrained by a constant
653 pressure of 1 bar, and the other models reflect ρ_w along the vapor and liquid branches of the steam
654 saturation curve (Fig. 10, see also Fig. 6b). These models demonstrate that density and cooling rate play
655 equally important roles in determining the temperature trajectory of α_{OBS} in volcanic emissions, and that
656 lower-density vapors and magmatic gases are more likely to preserve T maxima due to relatively sluggish
657 isotope exchange rates, combined with the fact that they cool more rapidly.

658 Natural geothermal pools have measured temperatures less than 100 °C (Fig. 10), and can be fed
659 by either steam/gas or liquid emissions (e.g., Lowenstern et al., 2012; Sheppard et al., 1992; Simmons et
660 al., 2005). For example, at Norris Basin in Yellowstone National Park (USA), the fluid T measured at the
661 point of sampling is ~ 90 °C (Welhan, 1981), having cooled from deeper, hotter conditions between 270
662 and 340 °C (Fournier, 1989). The dissolved chemistry indicates the fluids feeding Norris are liquids that
663 have undergone periodic boiling during upflow, and likely have lost a fraction of the deeper gas
664 component associated with steam separation (Fournier, 1989). In this case, it is reasonable to model
665 cooling using the T - ρ_w relationship of steam-saturated liquid, because the fluid is likely to follow the
666 boiling curve during upflow once intercepted (Ingebritsen et al., 2010). We assume minimal distillation
667 effects associated with boiling events because the equilibrium values for $\text{H}_{2(\text{aq})}$ – $\text{H}_{2(\text{g})}$ isotope fractionation
668 ($[\text{D}/\text{H}]_{\text{H}_{2(\text{aq})}} / [\text{D}/\text{H}]_{\text{H}_{2(\text{gas})}}$) are much smaller than equilibrium fractionation between H_2 and H_2O , especially
669 for $T > 100$ °C (see section 4.2, and Fig. S5). Using $\alpha_{\text{H}_2\text{O}(\text{L})-\text{H}_2(\text{AQ})}$ as the equilibrium reference, the best fit
670 gives a cooling rate of ~ 14 °C / hr (Fig. 10). Drill-hole measurements from Norris Basin indicate a T of
671 193 °C at 236 m depth (Bargar and Fournier, 1988), and from this information we derive an average flow

672 rate of ~32 m / hr, which is higher than the value calculated for Lost City (7 m / hr), but of the same
673 magnitude.

674 Isotope fractionation values (α_{OBS}) measured in liquids recovered from geothermal wells
675 generally show close agreement with equilibrium (Fig. 10). One way to test the validity of using simple
676 cooling models to constrain hydrological characteristics is to compare $\delta\text{D}_{\text{H}_2}$ measured in natural surface
677 emanations with those obtained from nearby geothermal wells. These wells often extend through lower
678 permeability cap rock and are fed from deeper formations of higher permeability, where convection in the
679 reservoir can produce a relatively uniform vertical temperature distribution on a scale of ~1 km (e.g.,
680 Arnórsson, 1995; Cox and Browne, 1998; Garcia et al., 2016). To first order we can conceptualize the
681 system as one where fluids come from a reservoir with a well-defined T that is sufficiently high that H_2
682 and H_2O are in isotopic equilibrium (typically 200–300 °C, $1/k_1 < 1.3$ hrs), and then cool as they pass
683 through the cap rock to the surface. The only such data currently available for comparison are from the
684 Ngawha geothermal field (NZ), and these appear somewhat anomalous (Lyon and Hulston, 1984),
685 precluding the development of useful kinetic models. The measured reservoir T at Ngawha is ~230 °C
686 (Cox and Browne, 1998; Giggenbach et al., 1993; Lyon and Hulston, 1984), whereas the α_{OBS} values of
687 well fluids and surface pools reflect minimum temperatures of ~440 °C and ~255 °C, respectively (Fig.
688 10). The difference between these two apparent temperatures is consistent with isotopic re-equilibration
689 as fluids cool during ascent through the cap rock, but it is difficult to explain how both values are higher
690 than the reservoir T . Temperatures exceeding 400 °C are reasonable at depths greater than typical
691 wellbores, having been measured in steam-dominated systems (Garcia et al., 2016). Ngawha, however, is
692 a liquid-dominated system (e.g., Simmons et al., 2016), and the water should boil/convect before
693 achieving such high T unless trapped in tight pore spaces at near-lithostatic pressure, meaning
694 permeability would be inherently low (Fournier, 1991, 1999; Johnson and Norton, 1991). These
695 constraints do not favor a scenario where gases have moved rapidly between a deeper (higher- T) source
696 region and the drilled reservoir (Lyon and Hulston, 1984). The unexpectedly high $\delta\text{D}_{\text{H}_2}$ measured also in
697 the Ngawha pools therefore warrants new field investigations here and in other geothermal systems to
698 compare isotope measurements between wells and surface emanations. This may be the best next step in
699 calibrating hydrological models that use D–H exchange kinetics to constrain permeability and flow rate in
700 hydrothermal systems.

701

702 **4.6. Implications for H_2 generated in low-temperature geologic settings**

703

704 The models developed in previous sections assume disequilibrium between $\delta\text{D}_{\text{H}_2}$ and $\delta\text{D}_{\text{H}_2\text{O}}$
705 observed in hydrothermal solutions largely results from passing through a steep temperature gradient,

706 where cooling occurs faster than the equilibration rate. The H₂ measured in continental shield gases and
 707 alkaline springs is likely generated at temperatures well below those driving hydrothermal convection,
 708 through processes like serpentinization. Any *T*-gradients experienced by these fluids will be
 709 comparatively mild, and α_{OBS} is typically closer to equilibrium at the *T* measured during sampling (Fig.
 710 1). However, potential kinetic isotope effects associated with H₂ generation become an important
 711 consideration with decreasing *T*, which could add uncertainty for cooling models applied in lower *T*
 712 settings. The term "kinetic isotope separation factor" (α_{KIE}) is often applied to the fractionation observed
 713 when new H₂ is formed from precursor H₂O ($\alpha_{\text{KIE}} = [\text{D}/\text{H}]_{\text{bulk H}_2\text{O}} / [\text{D}/\text{H}]_{\text{new H}_2}$), where α_{KIE} may not be
 714 equivalent to $\alpha_{\text{H}_2\text{O-H}_2(\text{eq})}$ at the *T* and *P* of formation. For example, if the $\delta\text{D}_{\text{H}_2}$ of newly-formed H₂ is out of
 715 equilibrium with $\delta\text{D}_{\text{H}_2\text{O}}$, and the associated *T* is sufficiently low that isotopic equilibration is sluggish,
 716 then the simplifying assumption that the kinetic cooling trajectory of α_{OBS} originated on the equilibrium
 717 curve ($\alpha_{\text{H}_2\text{O-H}_2(\text{eq})}$) is no longer valid (cf. Fig. 9).

718 Given kinetic isotope effects may be involved when H₂ is formed at low *T*, we can use our
 719 models to estimate maximum timeframes required to achieve isotopic equilibrium if we assume that H₂ is
 720 generated at a constant rate under isothermal conditions. Fluids containing dissolved H₂ liberated from
 721 fractures in Precambrian shield rock may represent the closest natural analogue to this scenario (Onstott et
 722 al., 2006; Sherwood Lollar et al., 1993a; Sherwood Lollar et al., 2007). Our models assume the α_{KIE}
 723 during radiolytic conversion of H₂O to H₂ observed by Lin et al. (2005), who proposed this as a potential
 724 mechanism for producing the H₂ observed in deep fracture fluids. They report $\alpha_{\text{KIE}} \approx 1.92$ at 25 °C,
 725 compared with $\alpha_{\text{H}_2\text{O(L)-H}_2(\text{AQ})} = 3.69$ (equilibrium, 25 °C), which means newly formed H₂ has a δD much
 726 higher than is expected for equilibrium the water. For the isothermal kinetic models we use equation 17 at
 727 *P* = 50 bars for the isotope exchange rates (*k*₁), which are effectively independent of the low H₂
 728 concentrations in natural fluids, and therefore an arbitrary H₂ generation rate may be used. The models
 729 simulate $d[\text{D}/\text{H}]_{\text{H}_2} / dt$ as accumulated (bulk) H₂ approaches equilibrium ($\alpha_{\text{H}_2\text{O(L)-H}_2(\text{AQ})}$), concurrent with
 730 the constant addition of new H₂ (where $\alpha_{\text{KIE}} = 1.92$). The results indicate maximum isothermal residence
 731 times (to 97% of equilibrium) of 1.3, 9 and 35 yrs at 50, 25, and 10 °C, respectively. We note, at these
 732 temperatures, 97% equates to $\delta\text{D}_{\text{H}_2}$ being ~8 ‰ from equilibrium, generally within the reproducibility of
 733 field samples.

734 Although α_{KIE} associated with serpentinization is unknown, currently available data do not
 735 suggest H₂ is likely to form any farther from isotopic equilibrium than the value proposed by Lin et al.
 736 (2005), either by abiotic or biological mechanisms (Hammerli et al., 1970; Krichevsky et al., 1961; Lin et
 737 al., 2005; Luo et al., 1991; Roy, 1962; Stojić et al., 1994; Topley and Eyring, 1934; Walter et al., 2012;
 738 Yang et al., 2012). Thus, in general, the timescales required to attain H₂-H₂O isotopic equilibrium in a
 739 liquid phase are insignificant relative to residence times of up to millions of years suggested for some

740 fracture fluids (Holland et al., 2013; Kietäväinen et al., 2014; Lippmann et al., 2003). Although, the
741 presence of a gas phase, if possible, would weaken this conclusion somewhat. Overall, isotope
742 fractionation (α_{OBS}) in Precambrian shield gases generally exhibits good agreement with equilibrium
743 (Fig. 1), especially when measured T is well constrained (Onstott et al., 2006).

744 Biological catalysis of D–H exchange may be another complicating factor in constraining kinetic
745 models of environments associated with low- T H_2 production. The utilization of H_2 is a prevalent
746 metabolic pathway in extreme chemical/physical environments, even where microbial productivity and
747 diversity are low (Brazelton et al., 2013; Colwell and D'Hondt, 2013; Lang et al., 2012; Lin et al., 2006;
748 Nealson et al., 2005; Onstott et al., 2006; Schrenk et al., 2004; Sherwood Lollar et al., 2007; Toki et al.,
749 2011). Cryogenic brine trapped beneath the permanent ice cover of Lake Vida in Antarctica provide an
750 interesting example of isotopic data from an extreme environment ($\delta\text{D}_{\text{H}_2} = -704$ ‰, $\delta\text{D}_{\text{H}_2\text{O}} = -250$ ‰ at -
751 13.4 °C). The $\delta\text{D}_{\text{H}_2}$ is far from equilibrium ($\alpha_{\text{OBS}} = 2.567$, Fig. 1) despite the presence of a (slow) bacterial
752 ecosystem (Murray et al., 2012). The brine appears to have been geochemically isolated for $\sim 2,800$ yrs,
753 and Murray et al. (2012) note the mechanism of H_2 production and the effect of microbes on C-H-N-S
754 isotope systematics are both poorly constrained. If we extend to -13.4 °C our model for estimating
755 maximum (isothermal) residence times, the results indicate $\delta\text{D}_{\text{H}_2}$ should reach equilibrium within ~ 350
756 yrs. This is shorter than the reported timeframe of isolation by an order of magnitude. Therefore, should
757 these Lake Vida data prove reproducible, the observed disequilibrium seems to require a mechanism of
758 H_2 removal that rivals the rate of production, and a kinetic isotope effect associated with this process. For
759 example, if we assume microbial activity only moves $\delta\text{D}_{\text{H}_2}$ towards equilibrium (Campbell et al., 2009;
760 Kawagucci et al., 2014; Okumura et al., 2016; Romanek et al., 2003; Valentine et al., 2004; Yang et al.,
761 2012), a low degree of biological activity may allow isotopically lighter H_2 to preferentially diffuse away
762 through the ice (Strauss et al., 1994). Thus, especially in cool or isolated geologic settings, representative
763 isotope exchange models may need to account for additional (physical) mechanisms that could impose
764 kinetic isotope separation, such as degassing or diffusion. In turn, such models might elucidate better the
765 impact of biology on D/H isotope systematics in extreme natural environments, with potential
766 implications for identifying bio-signatures elsewhere in the solar system.

767

768 5. CONCLUSIONS

769

770 Combining new and historical experimental data, we have derived a simple, but broadly
771 applicable rate law to describe the D–H exchange rate (k) between H_2 and H_2O as the system approaches
772 isotopic equilibrium. If species concentrations are cast in units of [mol/L], good agreement is observed
773 when comparing the results of liquid phase experiments, reported here, to those of gas phase experiments

774 previously reported by Lecluse and Robert (1994). First-order exchange rates (k_1 , units hr^{-1}) may be
775 calculated by constraining T and the concentrations $[\text{H}_2]$ and $[\text{H}_2\text{O}]$, both in mol/L, at the associated P of
776 interest. The result is a density-dependent rate expression that can easily account for phase changes that
777 commonly occur in evolving geological systems. The new experimental data also help constrain
778 equilibrium isotope fractionation for H_2 dissolved in liquid water, and we report updated polynomials to
779 describe the T dependence of $\alpha_{\text{H}_2\text{O}-\text{H}_2(\text{eq})}$ in the H_2 - H_2O system.

780 Isotope fractionation between H_2 and H_2O (α_{OBS}) is considered an important indicator of the
781 temperature history of naturally occurring fluids/gases. Historical field data concur with our
782 experimentally-derived rates, indicating D-H exchange kinetics are sufficiently fast in liquid water that
783 $\alpha_{\text{H}_2\text{O}-\text{H}_2}$ temperatures usually reflect equilibrium when T measured during sampling exceeds ~ 250 °C.
784 (e.g., Figs. 8). For liquid-phase solutions, such temperatures are below the near-critical limit of
785 hydrothermal convection. In such cases, as we have attempted to demonstrate, isotopic equilibrium ($\alpha_{\text{H}_2\text{O}-\text{H}_2(\text{eq})}$)
786 at these high-temperature conditions provides a relatively unambiguous starting point for simple
787 kinetic models that assume the degree of disequilibrium observed in natural fluids is a function of the
788 cooling rate. The H_2 - H_2O system appears uniquely sensitive in a temperature range ideal for estimating
789 transit times of upwardly-advecting hydrothermal solutions. Both T and density ($\sim \rho_w$) have a significant
790 effect on the D-H exchange rate, which explains the greater variability and relatively high $\alpha_{\text{H}_2\text{O}-\text{H}_2}$
791 temperatures reflected in steam discharges and fumarolic gases (e.g., Fig. 10).

792 Steep temperature gradients and relatively rapid cooling associated with hydrothermal convection
793 facilitate a greater degree of isotopic disequilibrium than is observed in alkaline spring waters and
794 Precambrian fracture fluids. In these systems, H_2 formation may occur at relatively low temperatures ($<$
795 100 °C), which increases the probability that factors other than cooling may have affected the observed
796 $\delta\text{D}_{\text{H}_2}$. When applied to hydrothermal fluids, kinetic cooling models indicate microbiomes must enhance
797 rates of isotopic re-equilibration at $T < \sim 60$ °C. In low- T discharges, where a high- T origin of H_2 cannot
798 be assumed, it is more difficult to demonstrate the biological effects. There is an additional possibility that
799 $\delta\text{D}_{\text{H}_2}$ can include a kinetic isotope effect associated with H_2 generation. In this case, disequilibrium could
800 be observed even if H_2 formed at the T measured during sampling, although our models suggest isotopic
801 equilibrium would be established within 1.3, 9 and 35 yrs at 50, 25, and 10 °C, respectively. BB

802 803 **ACKNOWLEDGEMENTS**

804
805 We would like to thank Daniel Stolper, Stuart Simmons, Ben Tutolo and Pat Dobson for
806 thoughtful discussions that contributed to the scope of the original manuscript. We also thank Matthew
807 Fantle and three anonymous reviewers, whose comments greatly improved the clarity and content of this
808 publication. This work was supported by the U.S. Department of Energy, Office of Science, Office of
809 Basic Energy Sciences, Chemical Sciences, Geosciences, and Biosciences Division, under Award
810 Number DE-AC02-05CH11231.

811

812 **REFERENCES**

- 813 Abrajano, T.A., Sturchio, N.C., Kennedy, B.M., Lyon, G.L., Muehlenbachs, K., Bohlke, J.K., 1990. Geochemistry
814 of reduced gas related to serpentinization of the Zambales ophiolite, Philippines. *Appl. Geochem.* 5, 625-630.
- 815 Ahlbom, K., Olsson, O., Sehlstedt, S., 1995. Temperature conditions in the SKB study sites. Svensk
816 Kärnbränslehantering AB, Tech. Rep. 95-16.
- 817 Albertsson, T., Semenov, D., Henning, T., 2014. Chemodynamical deuterium fractionation in the early solar nebula:
818 The origin of water on Earth and in asteroids and comets. *Astrophys. J.* 784, doi:10.1088/0004-
819 1637X/1784/1081/1039.
- 820 Allen, D.E., Seyfried, W.E., Jr., 2004. Serpentinization and heat generation: Constraints from Lost City and
821 Rainbow hydrothermal systems. *Geochim. Cosmochim. Acta* 68, 1347-1354.
- 822 Arnason, B., 1977. The hydrogen-water isotope thermometer applied to geothermal areas in Iceland. *Geothermics* 5,
823 75-80.
- 824 Arnason, B., Sigurgeirsson, T., 1968. Deuterium content of water vapor and hydrogen in volcanic gas at Surtsey,
825 Iceland. *Geochim. Cosmochim. Acta* 32, 807-813.
- 826 Arnórsson, S., 1995. Geothermal systems in Iceland: Structure and conceptual models—I. High-temperature areas.
827 *Geothermics* 24, 561-602.
- 828 Baker, E.T., German, C.R., 2004. On the global distribution of hydrothermal vent fields, in: German, C.R., Lin, J.,
829 Parson, L.M. (Eds.), *Mid-Ocean Ridges: Hydrothermal Interactions Between the Lithosphere and Oceans*, Geophys.
830 Monogr. Ser., 148. AGU, pp. 245-266.
- 831 Bardo, R.D., Wolfsberg, M., 1976. A theoretical calculation of the equilibrium constant for the isotopic exchange
832 reaction between H₂O and HD. *J. Phys. Chem.* 80, 1068-1071.
- 833 Bargar, K.E., Fournier, R.O., 1988. Effects of glacial ice on subsurface temperatures of hydrothermal systems in
834 Yellowstone National Park, Wyoming: Fluid-inclusion evidence. *Geology* 16, 1077-1080.
- 835 Barnes, I., O'Neil, J.R., Trescases, J.J., 1978. Present day serpentinization in New Caledonia, Oman and Yugoslavia.
836 *Geochim. Cosmochim. Acta* 42, 144-145.
- 837 Berndt, M.E., Allen, D.E., Seyfried, W.E., Jr., 1996a. Reduction of CO₂ during serpentinization of olivine at 300°C
838 and 500 bar. *Geology* 24, 351-354.
- 839 Berndt, M.E., Seal, R.R., II, Shanks, W.C., III, Seyfried, W.E., Jr., 1996b. Hydrogen isotope systematics of phase
840 separation in submarine hydrothermal systems: Experimental calibration and theoretical models. *Geochim.*
841 *Cosmochim. Acta* 60, 1595-1604.
- 842 Bischoff, J.L., 1991. Densities of liquids and vapors in boiling NaCl-H₂O solutions: A PVTx summary from 300° to
843 500°C. *Am. J. Sci.* 291, 309-338.
- 844 Bischoff, J.L., Rosenbauer, R.J., 1985. An empirical equation of state for hydrothermal seawater (3.2% NaCl). *Am.*
845 *J. Sci.* 285, 725-763.
- 846 Blackman, D.K., Karson, J.A., Kelley, D.S., Cann, J.R., Früh-Green, G.L., Gee, J.S., Hurst, S.D., John, B.E.,
847 Morgan, J., Nooner, S.L., Ross, D.K., Schroeder, T.J., Williams, E.A., 2002. *Geology of the Atlantis Massif (Mid-*

- 848 Atlantic Ridge, 30° N): Implications for the evolution of an ultramafic oceanic core complex. *Mar. Geophys. Res.*
849 23, 443-469.
- 850 Blackman, D.K., Slagle, A., Guerin, G., Harding, A., 2014. Geophysical signatures of past and present hydration
851 within a young oceanic core complex. *Geophys. Res. Lett.* 41, 1179-1186.
- 852 Boschi, C., Fruh-Green, G.L., Delacour, A., Karson, J.A., Kelley, D.S., 2006. Mass transfer and fluid flow during
853 detachment faulting and development of an oceanic core complex, Atlantis Massif (MAR 30°N). *Geochem.*
854 *Geophys. Geosyst.* 7, Q01004, doi: 01010.01029/02005GC001074.
- 855 Botz, R., Stüben, D., Winckler, G., Bayer, R., Schmitt, M., Faber, E., 1996. Hydrothermal gases offshore Milos
856 Island, Greece. *Chem. Geol.* 130, 161-173.
- 857 Brazelton, W.J., Morrill, P.L., Szponar, N., Schrenk, M.O., 2013. Bacterial communities associated with subsurface
858 geochemical processes in continental serpentinite springs. *Appl. Environ. Microbiol.* 79, 3906-3916.
- 859 Butterfield, D.A., Nakamura, K., Takano, B., Lilley, M.D., Lupton, J.E., Resing, J.A., Roe, K.K., 2011. High SO₂
860 flux, sulfur accumulation, and gas fractionation at an erupting submarine volcano. *Geology* 39, 803-806.
- 861 Campbell, B.J., Li, C., Sessions, A.L., Valentine, D.L., 2009. Hydrogen isotopic fractionation in lipid biosynthesis
862 by H₂-consuming *Desulfobacterium autotrophicum*. *Geochim. Cosmochim. Acta* 73, 2744-2757.
- 863 Cardace, D., Meyer-Dombard, D.A.R., Woycheese, K.M., Arcilla, C.A., 2015. Feasible metabolisms in high pH
864 springs of the Philippines. *Front. Microbiol.* 6, 10.
- 865 Charlou, J.L., Donval, J.P., Fouquet, Y., Jean-Baptiste, P., Holm, N., 2002. Geochemistry of high H₂ and CH₄ vent
866 fluids issuing from ultramafic rocks at the Rainbow hydrothermal field (36°14'N, MAR). *Chem. Geol.* 191, 345-359.
- 867 Chiodini, G., Marini, L., 1998. Hydrothermal gas equilibria: The H₂O-H₂-CO₂-CO-CH₄ system. *Geochim.*
868 *Cosmochim. Acta* 62, 2673-2687.
- 869 Cole, D.R., Chakraborty, S., 2001. Rates and mechanisms of isotopic exchange, in: Valley, J.W., Cole, D.R. (Eds.),
870 *Stable Isotope Geochemistry*, Rev. Mineral. Geochem. 43. MSA, Chantilly, VA, pp. 83-223.
- 871 Colwell, F.S., D'Hondt, S., 2013. Nature and extent of the deep biosphere, in: Hazen, R.M., Jones, A.P., Baross, J.A.
872 (Eds.), *Carbon in the Earth*, Rev. Min. Geochem. 75. MSA, pp. 547-574.
- 873 Coveney, R.M., Jr., Goebel, E.D., Zeller, E.J., Dreschhoff, G.A.M., Angino, E.E., 1987. Serpentinization and the
874 origin of hydrogen gas in Kansas. *Am. Assoc. Petr. Geol. B.* 71, 39-48.
- 875 Cox, M.E., Browne, P., 1998. Hydrothermal alteration mineralogy as an indicator of hydrology at the Ngawha
876 geothermal field, New Zealand. *Geothermics* 27, 259-270.
- 877 Craig, H., 1961. Standard for reporting concentrations of deuterium and oxygen-18 in natural waters. *Science* 133,
878 1833-1834.
- 879 Criss, R.E., 1999. *Principles of Stable Isotope Distribution*. Oxford University Press.
- 880 Criss, R.E., Gregory, R.T., Taylor, H.P., Jr., 1987. Kinetic theory of oxygen isotopic exchange between minerals and
881 water. *Geochim. Cosmochim. Acta* 51, 1099-1108.
- 882 D'Amore, F., Panichi, C., 1980. Evaluation of deep temperatures of hydrothermal systems by a new gas
883 geothermometer. *Geochim. Cosmochim. Acta* 44, 549-556.

- 884 Drummond, S.E., Ohmoto, H., 1985. Chemical evolution and mineral deposition in boiling hydrothermal systems.
885 *Econ. Geol.* 80, 126-147.
- 886 Edmond, J.M., Measures, C., McDuff, R.E., Chan, L., Collier, R., Grant, B., Gordon, L.I., Corliss, J., 1979. Ridge
887 crest hydrothermal activity and the balances of the major and minor elements in the ocean: The Galapagos data.
888 *Earth Planet. Sci. Lett.* 46, 1-18.
- 889 Etiopie, G., Samardzic, N., Grassa, F., Hrvatovic, H., Miosic, N., Skopljak, F., 2017. Methane and hydrogen in
890 hyperalkaline groundwaters of the serpentinized Dinaride ophiolite belt, Bosnia and Herzegovina. *Appl. Geochem.*
891 84, 286-296.
- 892 Fernandez-Prini, R., Alvarez, J.L., Harvey, A.H., 2003. Henry's constants and vapor-liquid distribution constants for
893 gaseous solutes in H₂O and D₂O at high temperatures. *J. Phys. Chem. Ref. Data* 32, 903-916.
- 894 Flournoy, J.M., Wilmarth, W.K., 1961. The base catalyzed exchange of hydrogen gas and protonic solvents. III. The
895 catalytic efficiency of concentrated aqueous alkali. *J. Am. Chem. Soc.* 83, 2257-2262.
- 896 Fournier, R.O., 1989. Geochemistry and dynamics of the Yellowstone National Park hydrothermal system. *Annu.*
897 *Rev. Earth Planet. Sci.* 17, 13-53.
- 898 Fournier, R.O., 1991. The transition from hydrostatic to greater than hydrostatic fluid pressure in presently active
899 continental hydrothermal systems in crystalline rock. *Geophys. Res. Lett.* 18, 955-958.
- 900 Fournier, R.O., 1999. Hydrothermal processes related to movement of fluid from plastic into brittle rock in the
901 magmatic-epithermal environment. *Econ. Geol.* 94, 1193-1211.
- 902 Foustoukos, D.I., Mysen, B.O., 2012. D/H fractionation in the H₂-H₂O system at supercritical water conditions:
903 Compositional and hydrogen bonding effects. *Geochim. Cosmochim. Acta* 86, 88-102.
- 904 Foustoukos, D.I., Savov, I.P., Janecky, D.R., 2008. Chemical and isotopic constraints on water/rock interactions at
905 the Lost City hydrothermal field, 30°N Mid-Atlantic Ridge. *Geochim. Cosmochim. Acta* 72, 5457-5474.
- 906 Friedman, I., 1953. Deuterium content of natural waters and other substances. *Geochim. Cosmochim. Acta* 4, 89-
907 103.
- 908 Friedman, I., O'Neil, J.R., 1977. Compilation of stable isotope fractionation factors of geochemical interest. *Data of*
909 *Geochemistry*, U.S. Geol. Surv. Prof. Paper 440-KK.
- 910 Fritz, P., Clark, I.D., Fontes, J.-C., Whiticar, M.J., Faber, E., 1992. Deuterium and ¹³C evidence for low temperature
911 production of hydrogen and methane in a highly alkaline groundwater environment in Oman, in: Kharaka, Y.K.,
912 Maest, A.S. (Eds.), *Proceed. 7th Intern. Symp. on Water-Rock Interaction: Low Temperature Environments.*
913 Balkema, Rotterdam, pp. 793-796.
- 914 Fu, Q., Lollar, B.S., Horita, J., Lacrampe-Couloume, G., Seyfried, W.E., Jr., 2007. Abiotic formation of
915 hydrocarbons under hydrothermal conditions: Constraints from chemical and isotope data. *Geochim. Cosmochim.*
916 *Acta* 71, 1982-1998.
- 917 Gallant, R.M., Von Damm, K.L., 2006. Geochemical controls on the hydrothermal fluids from the Kairei and
918 Edmond Vent Fields, 23°-25°S, Central Indian Ridge. *Geochem. Geophys. Geosyst.* 7, Q06018.
- 919 Garcia, J., Hartline, C., Walters, M., Wright, M., Rutqvist, J., Dobson, P.F., Jeanne, P., 2016. The Northwest
920 Geysers EGS Demonstration Project, California: Part 1: Characterization and reservoir response to injection.
921 *Geothermics* 63, 97-119.

- 922 Genda, H., Ikoma, M., 2008. Origin of the ocean on the Earth: Early evolution of water D/H in a hydrogen-rich
923 atmosphere. *Icarus* 194, 42-52.
- 924 German, C.R., Seyfried, W.E., Jr., 2014. Hydrothermal processes, in: Elias, S.A. (Ed.), *Treatise on Geochemistry*,
925 vol. 8: The Oceans and Marine Geochemistry. Elsevier, pp. 191-233.
- 926 Giggenbach, W.F., 1987. Redox processes governing the chemistry of fumarolic gas discharges from White Island,
927 New Zealand. *Appl. Geochem.* 2, 143-161.
- 928 Giggenbach, W.F., 1997. The origin and evolution of fluids in magmatic-hydrothermal systems, in: Barnes, H.L.
929 (Ed.), *Geochemistry of Hydrothermal Ore Deposits*, 3rd ed. John Wiley & Sons, Inc., pp. 737-796.
- 930 Giggenbach, W.F., Sano, Y., Wakita, H., 1993. Isotopic composition of helium, and CO₂ and CH₄ contents in gases
931 produced along the New Zealand part of a convergent plate boundary. *Geochim. Cosmochim. Acta* 57, 3427-3455.
- 932 Glover, R.B., Mroczek, E.K., 2009. Chemical changes in natural features and well discharges in response to
933 production at Wairakei, New Zealand. *Geothermics* 38, 117-133.
- 934 Gunter, B.D., Musgrave, B.C., 1971. New evidence on the origin of methane in hydrothermal gases. *Geochim.*
935 *Cosmochim. Acta* 35, 113-118.
- 936 Hammerli, M., Mislán, J.P., Olmstead, W.J., 1970. Effect of overpotential on the temperature dependence of the
937 electrolytic hydrogen-deuterium separation factor on platinum. *J. Electrochem. Soc.* 117, 751-757.
- 938 Harvey, M.C., Rowland, J.V., Chiodini, G., Rissmann, C.F., Bloomberg, S., Hernández, P.A., Mazot, A., Viveiros,
939 F., Werner, C., 2015. Heat flux from magmatic hydrothermal systems related to availability of fluid recharge. *J.*
940 *Volcanol. Geoth. Res.* 302, 225-236.
- 941 Haymon, R., 1983. Growth history of hydrothermal black smoker chimneys. *Nature* 301, 695-698.
- 942 Hilkert, A.W., Douthitt, C.B., Schlüter, H.J., Brand, W.A., 1999. Isotope ratio monitoring gas chromatography/mass
943 spectrometry of D/H by high temperature conversion isotope ratio mass spectrometry. *Rapid Commun. Mass*
944 *Spectrom.* 13, 1226-1230.
- 945 Holland, G., Lollar, B.S., Li, L., Lacrampe-Couloume, G., Slater, G.F., Ballentine, C.J., 2013. Deep fracture fluids
946 isolated in the crust since the Precambrian era. *Nature* 497, 357-360.
- 947 Horibe, Y., Craig, H., 1995. D/H fractionation in the system methane-hydrogen-water. *Geochim. Cosmochim. Acta*
948 59, 5209-5217.
- 949 Horita, J., Wesolowski, D.J., 1994. Liquid-vapor fractionation of oxygen and hydrogen isotopes of water from the
950 freezing to the critical temperature. *Geochim. Cosmochim. Acta* 58, 3425-3437.
- 951 Hsu, H.-W., Postberg, F., Sekine, Y., Shibuya, T., Kempf, S., Horányi, M., Juhász, A., Altobelli, N., Suzuki, K.,
952 Masaki, Y., Kuwatani, T., Tachibana, S., Sirono, S.-i., Moragas-Klostermeyer, G., Srama, R., 2015. Ongoing
953 hydrothermal activities within Enceladus. *Nature* 519, 207.
- 954 Ingebritsen, S.E., Geiger, S., Hurwitz, S., Driesner, T., 2010. Numerical simulation of magmatic hydrothermal
955 systems. *Rev. Geophys.* 48, RG1002, doi:10.1029/2009RG000287.
- 956 Jannasch, H.W., Mottl, M.J., 1985. Geomicrobiology of deep-sea hydrothermal vents. *Science* 229, 717-725.
- 957 Jeffrey, A.W.A., Kaplan, I.R., 1988. Hydrocarbons and inorganic gases in the Gravberg-1 well, Siljan Ring,
958 Sweden. *Chem. Geol.* 71, 237-255.

- 959 Jessop, A.M., Lewis, T., 1978. Heat flow and heat generation in the Superior Province of the Canadian Shield.
960 Tectonophysics 50, 55-77.
- 961 Johnson, J.W., Norton, D., 1991. Critical phenomena in hydrothermal systems: State, thermodynamic, electrostatic,
962 and transport properties of H₂O in the critical region. Am. J. Sci. 291, 541-648.
- 963 Juhlin, C., Wallroth, T., Smellie, J., Eliasson, T., Ljunggren, C., Leijon, B., Beswick, J., 1998. The very deep hole
964 concept: Geoscientific appraisal of conditions at great depth. Svensk Kärnbränslehantering AB, SKB-TR-98-05.
- 965 Kawagucci, S., 2015. Fluid geochemistry of high-temperature hydrothermal fields in the Okinawa Trough, in:
966 Ishibashi, J.-I., Okino, K., Sunamura, M. (Eds.), Subseafloor Biosphere Linked to Hydrothermal Systems: TAIGA
967 Concept. Springer, pp. 387-403.
- 968 Kawagucci, S., Chiba, H., Ishibashi, J.-I., Yamanaka, T., Toki, T., Muramatsu, Y., Ueno, Y., Makabe, A., Inoue, K.,
969 Yoshida, N., Nakagawa, S., Nunoura, T., Takai, K., Takahata, N., Sano, Y., Narita, T., Teranishi, G., Obata, H.,
970 Gamo, T., 2011. Hydrothermal fluid geochemistry at the Iheya North field in the mid-Okinawa Trough: Implication
971 for origin of methane in subseafloor fluid circulation systems. Geochim. J. 45, 109-124.
- 972 Kawagucci, S., Kobayashi, M., Hattori, S., Yamada, K., Ueno, Y., Takai, K., Yoshida, N., 2014. Hydrogen isotope
973 systematics among H₂-H₂O-CH₄ during the growth of the hydrogenotrophic methanogen *Methanothermobacter*
974 *thermautotrophicus* strain ΔH. Geochim. Cosmochim. Acta 142, 601-614.
- 975 Kawagucci, S., Miyazaki, J., Noguchi, T., Okamura, K., Shibuya, T., Watsuji, T., Nishizawa, M., Watanabe, H.,
976 Okino, K., Takahata, N., Sano, Y., Nakamura, K., Shuto, A., Abe, M., Takaki, Y., Nunoura, T., Koonjul, M., Singh,
977 M., Beedessee, G., Khishma, M., Bhoyroo, V., Bissessur, D., Kumar, L.S., Marie, D., Tamaki, K., Takai, K., 2016.
978 Fluid chemistry in the Solitaire and Dodo hydrothermal fields of the Central Indian Ridge. Geofluids 16, doi:
979 10.1111/gfl.12201.
- 980 Kawagucci, S., Toki, T., Ishibashi, J.-I., Takai, K., Ito, M., Oomori, T., Gamo, T., 2010. Isotopic variation of
981 molecular hydrogen in 20°–375°C hydrothermal fluids as detected by a new analytical method. J. Geophys. Res.
982 115, G03021, doi:03010.01029/02009JG001203.
- 983 Kelley, D.S., Baross, J.A., Delaney, J.R., 2002. Volcanoes, Fluids, and Life at Mid-Ocean Ridge Spreading Centers.
984 Annu. Rev. Earth Planet. Sci. 30, 385-491.
- 985 Kelley, D.S., Karson, J.A., Blackman, D.K., Fruh-Green, G.L., Butterfield, D.A., Lilley, M.D., Olson, E.J., Schrenk,
986 M.O., Roe, K.K., Lebon, G.T., Rivizzigno, P., 2001. An off-axis hydrothermal vent field near the Mid-Atlantic
987 Ridge at 30°N. Nature 412, 145-149.
- 988 Kelley, D.S., Karson, J.A., Früh-Green, G.L., Yoerger, D.R., Shank, T.M., Butterfield, D.A., Hayes, J.M., Schrenk,
989 M.O., Olson, E.J., Proskurowski, G., Jakuba, M., Bradley, A., Larson, B., Ludwig, K., Glickson, D., Buckman, K.,
990 Bradley, A.S., Brazelton, W.J., Roe, K., Elend, M.J., Delacour, A., Bernasconi, S.M., Lilley, M.D., Baross, J.A.,
991 Summons, R.E., Sylva, S.P., 2005. A serpentinite-hosted ecosystem: The Lost City hydrothermal field. Science 307,
992 1428-1434.
- 993 Kietäväinen, R., Ahonen, L., Kukkonen, I.T., Niedermann, S., Wiersberg, T., 2014. Noble gas residence times of
994 saline waters within crystalline bedrock, Outokumpu Deep Drill Hole, Finland. Geochim. Cosmochim. Acta 145,
995 159-174.
- 996 Kietäväinen, R., Ahonen, L., Niinikoski, P., Nykänen, H., Kukkonen, I.T., 2017. Abiotic and biotic controls on
997 methane formation down to 2.5 km depth within the Precambrian Fennoscandian Shield. Geochim. Cosmochim.
998 Acta 202, 124-145.
- 999 Kim, J., Sonnenthal, E., Rutqvist, J., 2015. A sequential implicit algorithm of chemo-thermo-poro-mechanics for
1000 fractured geothermal reservoirs. Comp. Geosci. 76, 59-71.

- 1001 Kishima, N., 1989. A thermodynamic study on the pyrite-pyrrhotite-magnetite-water system at 300–500°C with
1002 relevance to the fugacity/concentration quotient of aqueous H₂S. *Geochim. Cosmochim. Acta* 53, 2143-2155.
- 1003 Kishima, N., Sakai, H., 1984. Fugacity-concentration relationship of dilute hydrogen in water at elevated
1004 temperature and pressure. *Earth Planet. Sci. Lett.* 67, 79-86.
- 1005 Kita, A., Matsuo, S., Wakita, H., Nakamura, Y., 1980. D/H ratios of H₂ in soil gases as an indicator of fault
1006 movements. *Geochem. J.* 14, 317-320.
- 1007 Kiyosu, Y., 1983. Hydrogen isotopic compositions of hydrogen and methane from some volcanic areas in
1008 northeastern Japan. *Earth Planet. Sci. Lett.* 62, 41-52.
- 1009 Kiyosu, Y., Okamoto, Y., 1998. Variation in fumarolic H₂ gas and volcanic activity at Nasudake in Japan. *J.*
1010 *Volcanol. Geoth. Res.* 80, 27-37.
- 1011 Klein, F., Grozeva, N.G., Seewald, J.S., McCollom, T.M., Humphris, S.E., Moskowicz, B., Berquó, T.S., Kahl, W.-
1012 A., 2015. Experimental constraints on fluid-rock reactions during incipient serpentinization of harzburgite. *Am.*
1013 *Mineral.* 100, 991-1002.
- 1014 Knox, M., Quay, P.D., Wilbur, D., 1992. Kinetic isotopic fractionation during air-water gas transfer of O₂, N₂, CH₄,
1015 and H₂. *J. Geophys. Res.* 97, 20335-20343.
- 1016 Komor, S.C., Valley, J.W., Brown, P.E., 1988. Fluid-inclusion evidence for impact heating at the Siljan Ring,
1017 Sweden. *Geology* 16, 711-715.
- 1018 Konn, C., Donval, J.P., Guyader, V., Roussel, E., Fourre, E., Jean-Baptiste, P., Pelleter, E., Charlou, J.L., Fouquet,
1019 Y., 2018. Organic, gas, and element geochemistry of hydrothermal fluids of the newly discovered extensive
1020 hydrothermal area in the Wallis and Futuna region (SW Pacific). *Geofluids* 2018, doi: 10.1155/2018/7692839.
- 1021 Konno, U., Tsunogai, U., Nakagawa, F., Nakaseama, M., Ishibashi, J.-i., Nunoura, T., Nakamura, K.-i., 2006. Liquid
1022 CO₂ venting on the seafloor: Yonaguni Knoll IV hydrothermal system, Okinawa Trough. *Geophys. Res. Lett.* 33,
1023 L16607, doi:10.1029/2006GL026115.
- 1024 Krichevsky, M.I., Friedman, I., Newell, M.F., Sisler, F.D., 1961. Deuterium fractionation during molecular
1025 hydrogen formation in a marine pseudomonad. *J. Biol. Chem.* 236, 2520-2525.
- 1026 Lang, S.Q., Früh-Green, G.L., Bernasconi, S.M., Lilley, M.D., Proskurowski, G., Méhay, S., Butterfield, D.A.,
1027 2012. Microbial utilization of abiogenic carbon and hydrogen in a serpentinite-hosted system. *Geochim.*
1028 *Cosmochim. Acta* 92, 82-99.
- 1029 Lasaga, A.C., 1998. *Kinetic Theory in Earth Sciences*. Princeton University Press.
- 1030 Lecluse, C., Robert, F., 1994. Hydrogen isotope exchange reaction rates: Origin of water in the inner solar system.
1031 *Geochim. Cosmochim. Acta* 58, 2927-2939.
- 1032 Lemke, K.H., Rosenbauer, R.J., Bird, D.K., 2009. Peptide synthesis in early Earth hydrothermal systems.
1033 *Astrobiology* 9, 141-146.
- 1034 Lilley, M.D., Lupton, J.E., Butterfield, D.A., Olson, E., 2003. Magmatic events can produce rapid changes in
1035 hydrothermal vent chemistry. *Nature* 422, 878-881.
- 1036 Lin, L.-H., Slater, G.F., Sherwood Lollar, B., Lacrampe-Couloume, G., Onstott, T.C., 2005. The yield and isotopic
1037 composition of radiolytic H₂, a potential energy source for the deep subsurface biosphere. *Geochim. Cosmochim.*
1038 *Acta* 69, 893-903.

- 1039 Lin, L.-H., Wang, P.-L., Rumble, D., Lippmann-Pipke, J., Boice, E., Pratt, L.M., Lollar, B.S., Brodie, E.L., Hazen,
1040 T.C., Andersen, G.L., DeSantis, T.Z., Moser, D.P., Kershaw, D., Onstott, T.C., 2006. Long-term sustainability of a
1041 high-energy, low-diversity crustal biome. *Science* 314, 479-482.
- 1042 Lippmann, J., Stute, M., Torgersen, T., Moser, D.P., Hall, J.A., Lin, L., Borcsik, M., Bellamy, R.E.S., Onstott, T.C.,
1043 2003. Dating ultra-deep mine waters with noble gases and ³⁶Cl, Witwatersrand Basin, South Africa. *Geochim.*
1044 *Cosmochim. Acta* 67, 4597-4619.
- 1045 Lowenstern, J.B., Bergfeld, D., Evans, W.C., Hurwitz, S., 2012. Generation and evolution of hydrothermal fluids at
1046 Yellowstone: Insights from the Heart Lake Geyser Basin. *Geochem. Geophys. Geosyst.* 13, Q01017,
1047 doi:10.1029/2011GC003835.
- 1048 Luo, Y.-H., Sternberg, L., Suda, S., Kumazawa, S., Mitsui, A., 1991. Extremely low D/H ratios of photoproduced
1049 hydrogen by cyanobacteria. *Plant Cell Physiol.* 32, 897-900.
- 1050 Lupton, J., Butterfield, D., Lilley, M., Evans, L., Nakamura, K.-i., Chadwick, W., Resing, J., Embley, R., Olson, E.,
1051 Proskurowski, G., Baker, E., de Ronde, C., Roe, K., Greene, R., Lebon, G., Young, C., 2006. Submarine venting of
1052 liquid carbon dioxide on a Mariana Arc volcano. *Geochem. Geophys. Geosyst.* 7, Q08007,
1053 doi:10.1029/2005GC001152.
- 1054 Lyon, G.L., Hulston, J.R., 1984. Carbon and hydrogen isotopic compositions of New Zealand geothermal gases.
1055 *Geochim. Cosmochim. Acta* 48, 1161-1171.
- 1056 Marsic, N., Grundfelt, B., 2013. Review of geoscientific data of relevance to disposal of spent nuclear fuel in deep
1057 boreholes in crystalline rock. *Svensk Kärnbränslehantering AB, SKB-P-13-12.*
- 1058 Mayhew, L.E., Ellison, E.T., McCollom, T.M., Trainor, T.P., Templeton, A.S., 2013. Hydrogen generation from
1059 low-temperature water-rock reactions. *Nat. Geosci.* 6, 478-484.
- 1060 McCollom, T.M., Klein, F., Robbins, M., Moskowitz, B., Berquó, T.S., Jöns, N., Bach, W., Templeton, A., 2016.
1061 Temperature trends for reaction rates, hydrogen generation, and partitioning of iron during experimental
1062 serpentinization of olivine. *Geochim. Cosmochim. Acta* 181, 175-200.
- 1063 McDermott, J.M., Seewald, J.S., German, C.R., Sylva, S.P., 2015. Pathways for abiotic organic synthesis at
1064 submarine hydrothermal fields. *Proc. Natl. Acad. Sci. U.S.A.* 112, 7668-7672.
- 1065 McDermott, J.M., Sylva, S.P., Ono, S., German, C.R., Seewald, J.S., 2018. Geochemistry of fluids from Earth's
1066 deepest ridge-crest hot-springs: Piccard hydrothermal field, Mid-Cayman Rise. *Geochim. Cosmochim. Acta* 228,
1067 95-118.
- 1068 Miller, H.M., Matter, J.M., Kelemen, P., Ellison, E.T., Conrad, M.E., Fierer, N., Ruchala, T., Tominaga, M.,
1069 Templeton, A.S., 2016. Modern water/rock reactions in Oman hyperalkaline peridotite aquifers and implications for
1070 microbial habitability. *Geochim. Cosmochim. Acta* 179, 217-241.
- 1071 Miller, S.L., Rittenberg, D., 1958. The Catalysis of the H₂-D₂O exchange by aqueous buffer solutions. *J. Am. Chem.*
1072 *Soc.* 80, 64-65.
- 1073 Mizutani, Y., 1983. Deuterium fractionation between water vapor and hydrogen gas in fumarolic gases. *Geochem. J.*
1074 17, 161-164.
- 1075 Morrison, J., Brockwell, T., Merren, T., Fourel, F., Phillips, A.M., 2001. On-line high-precision stable hydrogen
1076 isotopic analyses on nanoliter water samples. *Anal. Chem.* 73, 3570-3575.
- 1077 Muccitelli, J., Wen, W.-Y., 1978. Solubilities of hydrogen and deuterium gases in water and their isotope
1078 fractionation factor. *J. Sol. Chem.* 7, 257-267.

- 1079 Murray, A.E., Kenig, F., Fritsen, C.H., McKay, C.P., Cawley, K.M., Edwards, R., Kuhn, E., McKnight, D.M.,
1080 Ostrom, N.E., Peng, V., Ponce, A., Priscu, J.C., Samarkin, V., Townsend, A.T., Wagh, P., Young, S.A., Yung, P.T.,
1081 Doran, P.T., 2012. Microbial life at -13°C in the brine of an ice-sealed Antarctic lake. *Proc. Natl. Acad. Sci. U.S.A.*
1082 109, 20626-20631.
- 1083 Neal, C., Stanger, G., 1983. Hydrogen generation from mantle source rocks in Oman. *Earth Planet. Sci. Lett.* 66,
1084 315-320.
- 1085 Nealson, K.H., Inagaki, F., Takai, K., 2005. Hydrogen-driven subsurface lithoautotrophic microbial ecosystems
1086 (SLiMEs): do they exist and why should we care? *Trends Microbiol.* 13, 405-410.
- 1087 Niemann, H.B., Atreya, S.K., Demick, J.E., Gautier, D., Haberman, J.A., Harpold, D.N., Kasprzak, W.T., Lunine,
1088 J.I., Owen, T.C., Raulin, F., 2010. Composition of Titan's lower atmosphere and simple surface volatiles as
1089 measured by the Cassini-Huygens probe gas chromatograph mass spectrometer experiment. *J. Geophys. Res.* 115,
1090 E12006, doi: 2010.1029/2010JE003659.
- 1091 Okumura, T., Kawagucci, S., Saito, Y., Matsui, Y., Takai, K., Imachi, H., 2016. Hydrogen and carbon isotope
1092 systematics in hydrogenotrophic methanogenesis under H_2 -limited and H_2 -enriched conditions: implications for the
1093 origin of methane and its isotopic diagnosis. *Prog. Earth Planet. Sci.* 3, doi: 10.1186/s40645-40016-40088-40643.
- 1094 Onstott, T.C., Lin, L.-H., Davidson, M., Mislouack, B., Borcsik, M., Hall, J., Slater, G., Ward, J., Sherwood Lollar,
1095 B., Lippmann-Pipke, J., Boice, E., Pratt, L.M., Pfiffner, S., Moser, D., Gihring, T., Kieft, T.L., Phelps, T.J.,
1096 Vanheerden, E., Litthaur, D., Deflaun, M., Rothmel, R., Wanger, G., Southam, G., 2006. The origin and age of
1097 biogeochemical trends in deep fracture water of the Witwatersrand Basin, South Africa. *Geomicrobiol. J.* 23, 369-
1098 414.
- 1099 Orcutt, B.N., Sylvan, J.B., Knab, N.J., Edwards, K.J., 2011. Microbial ecology of the dark ocean above, at, and
1100 below the seafloor. *Microbiol. Mol. Biol. Rev.* 75, 361-422.
- 1101 Palmer, D.A., Drummond, S.E., 1986. Thermal decarboxylation of acetate. Part I. The kinetics and mechanism of
1102 reaction in aqueous solution. *Geochim. Cosmochim. Acta* 50, 813-823.
- 1103 Pester, N.J., Butterfield, D.A., Foustoukos, D.I., Roe, K.K., Ding, K., Shank, T.M., Seyfried, W.E., Jr., 2008. The
1104 chemistry of diffuse-flow vent fluids on the Galapagos Rift (86°W): Temporal variability and seafloor phase
1105 equilibria controls, in: Lowell, R.P., Seewald, J.S., Perfit, M.R., Metaxas, A. (Eds.), *Magma to Microbe: Modeling*
1106 *Hydrothermal Processes at Oceanic Spreading Centers*, Geophys. Monogr. Ser., 178. AGU, Washington, D.C., pp.
1107 123-144.
- 1108 Pester, N.J., Ding, K., Seyfried, W.E., Jr., 2014. Magmatic eruptions and iron volatility in deep-sea hydrothermal
1109 fluids. *Geology* 42, 255-258.
- 1110 Pester, N.J., Rough, M., Ding, K., Seyfried, W.E., Jr., 2011. A new Fe/Mn geothermometer for hydrothermal
1111 systems: Implications for high-salinity fluids at 13°N on the East Pacific Rise. *Geochim. Cosmochim. Acta* 75,
1112 7881-7892.
- 1113 Proskurowski, G., Lilley, M.D., Kelley, D.S., Olson, E.J., 2006. Low temperature volatile production at the Lost
1114 City Hydrothermal Field, evidence from a hydrogen stable isotope geothermometer. *Chem. Geol.* 229, 331-343.
- 1115 Reeves, E.P., Seewald, J.S., Saccocia, P.J., Bach, W., Craddock, P.R., Shanks, W.C., Sylva, S.P., Walsh, E., Pichler,
1116 T., Rosner, M., 2011. Geochemistry of hydrothermal fluids from the PACMANUS, Northeast Pual and Vienna
1117 Woods hydrothermal fields, Manus Basin, Papua New Guinea. *Geochim. Cosmochim. Acta* 75, 1088-1123.
- 1118 Reeves, E.P., Seewald, J.S., Sylva, S.P., 2012. Hydrogen isotope exchange between *n*-alkanes and water under
1119 hydrothermal conditions. *Geochim. Cosmochim. Acta* 77, 582-599.

- 1120 Reysenbach, A.-L., Liu, Y., Banta, A.B., Beveridge, T.J., Kirshtein, J.D., Schouten, S., Tivey, M.K., Von Damm,
1121 K.L., Voytek, M.A., 2006. A ubiquitous thermoacidophilic archaeon from deep-sea hydrothermal vents. *Nature*
1122 442, 444-447.
- 1123 Richet, P., Bottinga, Y., Javoy, M., 1977. A review of hydrogen, carbon, nitrogen, oxygen, sulphur, and chlorine
1124 stable isotope fractionation among gaseous molecules. *Annu. Rev. Earth Planet. Sci.* 5, 65-110.
- 1125 Robert, F., Gautier, D., Dubrulle, B., 2000. The solar system D/H ratio: Observations and theories. *Space Sci. Rev.*
1126 92, 201-224.
- 1127 Romanek, C.S., Zhang, C.L., Li, Y., Horita, J., Vali, H., Cole, D.R., Phelps, T.J., 2003. Carbon and hydrogen
1128 isotope fractionations associated with dissimilatory iron-reducing bacteria. *Chem. Geol.* 195, 5-16.
- 1129 Roy, L.P., 1962. Influence of temperature on the electrolytic separation factor of hydrogen isotopes. *Can. J. Chem.*
1130 40, 1452-1460.
- 1131 Schmidt, K., Koschinsky, A., Garbe-Schonberg, D., de Carvalho, L.M., Seifert, R., 2007. Geochemistry of
1132 hydrothermal fluids from the ultramafic-hosted Logatchev hydrothermal field, 15°N on the Mid-Atlantic Ridge:
1133 Temporal and spatial investigation. *Chem. Geol.* 242, 1-21.
- 1134 Schrenk, M.O., Kelley, D.S., Bolton, S.A., Baross, J.A., 2004. Low archaeal diversity linked to seafloor
1135 geochemical processes at the Lost City Hydrothermal Field, Mid-Atlantic Ridge. *Environ. Microbiol.* 6, 1086-1095.
- 1136 Scott, S., Driesner, T., Weis, P., 2015. Geologic controls on supercritical geothermal resources above magmatic
1137 intrusions. *Nat. Comm.* 6, 7837, doi: 7810.1038/ncomms8837.
- 1138 Scott, S., Gunnarsson, I., Arnórsson, S., Stefánsson, A., 2014. Gas chemistry, boiling and phase segregation in a
1139 geothermal system, Hellisheidi, Iceland. *Geochim. Cosmochim. Acta* 124, 170-189.
- 1140 Seewald, J., Cruse, A., Saccocia, P., 2003. Aqueous volatiles in hydrothermal fluids from the Main Endeavour Field,
1141 northern Juan de Fuca Ridge: Temporal variability following earthquake activity. *Earth Planet. Sci. Lett.* 216, 575-
1142 590.
- 1143 Seewald, J.S., Seyfried, W.E., Jr., 1990. The effect of temperature on metal mobility in seafloor hydrothermal
1144 systems: Constraints from basalt alteration experiments. *Earth Planet. Sci. Lett.* 101, 388-403.
- 1145 Seward, T.M., Kishima, N., 1987. Problems in working with hydrogen under hydrothermal, in: Ulmer, G.C., Barnes,
1146 H.L. (Eds.), *Hydrothermal Experimental Techniques*. Wiley Interscience, pp. 141-156.
- 1147 Seyfried, W.E., Jr., 1987. Experimental and theoretical constraints on hydrothermal alteration processes at mid-
1148 ocean ridges. *Annu. Rev. Earth Planet. Sci.* 15, 317-335.
- 1149 Seyfried, W.E., Jr., Ding, K., 1995. Phase equilibria in seafloor hydrothermal systems: A review of the role of
1150 redox, temperature, pH and dissolved Cl on the chemistry of hot spring fluids at mid-ocean ridges, in: Humphris,
1151 S.E., Zierenberg, R.A., Mullineaux, L.S., Thompson, R.E. (Eds.), *Seafloor Hydrothermal Systems: Physical,
1152 Chemical, Biological and Geological Interactions*, Geophys. Monogr. Ser., 91. AGU, Washington, D.C., pp. 248-
1153 273.
- 1154 Seyfried, W.E., Jr., Ding, K., Berndt, M.E., 1991. Phase equilibria constraints on the chemistry of hot spring fluids
1155 at mid-ocean ridges. *Geochim. Cosmochim. Acta* 55, 3559-3580.
- 1156 Seyfried, W.E., Jr., Foustoukos, D.I., Fu, Q., 2007. Redox evolution and mass transfer during serpentinization: An
1157 experimental and theoretical study at 200°C, 500 bar with implications for ultramafic-hosted hydrothermal systems
1158 at mid-ocean ridges. *Geochim. Cosmochim. Acta* 71, 3872-3886.

- 1159 Seyfried, W.E., Jr., Gordon, P.C., Dickson, F.W., 1979. A new reaction cell for hydrothermal solution equipment.
1160 *Am. Mineral.* 64, 646-649.
- 1161 Seyfried, W.E., Jr., Janecky, D.R., Berndt, M.E., 1987. Rocking autoclaves for hydrothermal experiments II: The
1162 flexible reaction-cell system, in: Ulmer, G.C., Barnes, H.L. (Eds.), *Hydrothermal Experimental Techniques*. Wiley
1163 Interscience, pp. 216-239.
- 1164 Seyfried, W.E., Jr., Pester, N., Qi, F., 2010. Phase equilibria controls on the chemistry of vent fluids from
1165 hydrothermal systems on slow spreading ridges: Reactivity of plagioclase and olivine solid solutions and the pH-
1166 silica connection, in: Rona, P.A., Devey, C.W., Dymont, J., Murton, B.J. (Eds.), *Diversity of Hydrothermal Systems*
1167 *on Slow Spreading Ocean Ridges*, *Geophys. Monogr. Ser.* 188. AGU, Washington, D.C., pp. 297-320.
- 1168 Seyfried, W.E., Jr., Pester, N.J., Ding, K., Rough, M., 2011. Vent fluid chemistry of the Rainbow hydrothermal
1169 system (36°N, MAR): Phase equilibria and in-situ pH controls on seafloor alteration processes. *Geochim.*
1170 *Cosmochim. Acta* 75, 1574-1593.
- 1171 Seyfried, W.E., Jr., Pester, N.J., Tutolo, B.M., Ding, K., 2015. The Lost City hydrothermal system: Constraints
1172 imposed by vent fluid chemistry and reaction path models on seafloor heat and mass transfer processes.
1173 *Geochim. Cosmochim. Acta* 163, 59-79.
- 1174 Shanks, W.C., III, 2001. Stable isotopes in seafloor hydrothermal systems: Vent fluids, hydrothermal deposits,
1175 hydrothermal alteration, and microbial processes, in: Valley, J.W., Cole, D.R. (Eds.), *Stable Isotope Geochemistry*,
1176 *Rev. Mineral. Geochem.* 43. MSA, pp. 469-526.
- 1177 Sheppard, D.S., Truesdell, A.H., Janik, C.J., 1992. Geothermal gas compositions in Yellowstone National Park,
1178 USA. *J. Volcanol. Geoth. Res.* 51, 79-93.
- 1179 Sherwood Lollar, B., Frapé, S.K., Fritz, P., Macko, S.A., Welhan, J.A., Blomqvist, R., Lahermo, P.W., 1993a.
1180 Evidence for bacterially generated hydrocarbon gas in Canadian shield and fennoscandian shield rocks. *Geochim.*
1181 *Cosmochim. Acta* 57, 5073-5085.
- 1182 Sherwood Lollar, B., Frapé, S.K., Weise, S.M., Fritz, P., Macko, S.A., Welhan, J.A., 1993b. Abiogenic
1183 methanogenesis in crystalline rocks. *Geochim. Cosmochim. Acta* 57, 5087-5097.
- 1184 Sherwood Lollar, B., Lacrampe-Couloume, G., Voglesonger, K., Onstott, T.C., Pratt, L.M., Slater, G.F., 2008.
1185 Isotopic signatures of CH₄ and higher hydrocarbon gases from Precambrian Shield sites: A model for abiogenic
1186 polymerization of hydrocarbons. *Geochim. Cosmochim. Acta* 72, 4778-4795.
- 1187 Sherwood Lollar, B., Voglesonger, K., Lin, L.-H., Lacrampe-Couloume, G., Telling, J., Abrajano, T.A., Onstott,
1188 T.C., Pratt, L.M., 2007. Hydrogeologic controls on episodic H₂ release from precambrian fractured rocks—Energy
1189 for deep subsurface life on Earth and Mars. *Astrobiology* 7, 971-986.
- 1190 Shock, E.L., 1992. Chemical environments of submarine hydrothermal systems. *Origins Life Evol. Biosphere* 22,
1191 67-107.
- 1192 Simmons, S.F., Brown, K.L., Tutolo, B.M., 2016. Hydrothermal transport of Ag, Au, Cu, Pb, Te, Zn, and other
1193 metals and metalloids in New Zealand geothermal systems: Spatial patterns, fluid-mineral equilibria, and
1194 implications for epithermal mineralization. *Econ. Geol.* 111, 589-618.
- 1195 Simmons, S.F., Harris, S.P., Cassidy, J., 2005. Lake-filled depressions resulting from cold gas discharge in the
1196 Ngawha Geothermal Field, New Zealand. *J. Volcanol. Geoth. Res.* 147, 329-341.
- 1197 Sleep, N.H., Meibom, A., Fridriksson, T., Coleman, R.G., Bird, D.K., 2004. H₂-rich fluids from serpentinization:
1198 Geochemical and biotic implications. *Proc. Natl. Acad. Sci. U.S.A.* 101, 12818-12823.

- 1199 Spycher, N.F., Reed, M.H., 1988. Fugacity coefficients of H₂, CO₂, CH₄, H₂O and of H₂O-CO₂-CH₄ mixtures: A
1200 virial equation treatment for moderate pressures and temperatures applicable to calculations of hydrothermal boiling.
1201 *Geochim. Cosmochim. Acta* 52, 739-749.
- 1202 Stojić, D.L., Miljanić, Š.S., Grozdić, T.D., Golobočanin, D.D., Sovili, S.P., Jakšić, M.M., 1994. D/H isotope
1203 separation efficiency in water electrolysis. Improvement by in situ activation at different temperatures. *Int. J.*
1204 *Hydrogen Energy* 19, 587-590.
- 1205 Strauss, H.L., Chen, Z., Loong, C.-K., 1994. The diffusion of H₂ in hexagonal ice at low temperatures. *J. Chem.*
1206 *Phys.* 101, 7177-7180.
- 1207 Suda, K., Ueno, Y., Yoshizaki, M., Nakamura, H., Kurokawa, K., Nishiyama, E., Yoshino, K., Hongoh, Y.,
1208 Kawachi, K., Omori, S., Yamada, K., Yoshida, N., Maruyama, S., 2014. Origin of methane in serpentinite-hosted
1209 hydrothermal systems: The CH₄-H₂-H₂O hydrogen isotope systematics of the Hakuba Happo hot spring. *Earth*
1210 *Planet. Sci. Lett.* 386, 112-125.
- 1211 Suess, H.E., 1949. Das Gleichgewicht $H_2 + HDO \rightleftharpoons HD + H_2O$ und die weiteren austauschgleichgewichte im system
1212 H₂, D₂ und H₂O. *Z. Naturforsch.* 4, 328-332.
- 1213 Symons, E.A., Buncel, E., 1973. Base-catalyzed isotopic exchange of molecular hydrogen. II. Rate dependence on
1214 basicity in the dimethyl sulfoxide-water system. *Can. J. Chem.* 51, 1673-1681.
- 1215 Taran, Y.A., Pilipenko, V.P., Rozhkov, A.M., Vakin, E.A., 1992. A geochemical model for fumaroles of the
1216 Mutnovsky volcano, Kamchatka, USSR. *J. Volcanol. Geoth. Res.* 49, 269-283.
- 1217 Taran, Y.A., Varley, N.R., Inguaggiato, S., Cienfuegos, E., 2010. Geochemistry of H₂- and CH₄-enriched
1218 hydrothermal fluids of Socorro Island, Revillagigedo Archipelago, Mexico. Evidence for serpentinitization and
1219 abiogenic methane. *Geofluids* 10, 542-555.
- 1220 Titarenko, S.S., McCaig, A.M., 2016. Modelling the Lost City hydrothermal field: influence of topography and
1221 permeability structure. *Geofluids* 16, 314-328.
- 1222 Tivey, M.K., Olson, L.O., Miller, V.W., Light, R.D., 1990. Temperature measurements during initiation and growth
1223 of a black smoker chimney. *Nature* 346, 51-54.
- 1224 Tobias, H.J., Goodman, K.J., Blacken, C.E., Brenna, J.T., 1995. High-precision D/H measurement from hydrogen
1225 gas and water by continuous-flow isotope ratio mass spectrometry. *Anal. Chem.* 67, 2486-2492.
- 1226 Toki, T., Maegawa, K., Tsunogai, U., Kawagucci, S., Takahata, N., Sano, Y., Ashi, J., Kinoshita, M., Gamo, T.,
1227 2011. Gas chemistry of pore fluids from Oomine Ridge on the Nankai accretionary prism, in: Ogawa, Y., Anma, R.,
1228 Dilek, Y. (Eds.), *Accretionary Prisms and Convergent Margin Tectonics in the Northwest Pacific Basin*, *Mod. Appr.*
1229 *Sol. Earth Sci.* v8, pp. 247-262.
- 1230 Topley, B., Eyring, H., 1934. The separation of the hydrogen isotopes by electrolysis. Part I. *J. Chem. Phys.* 2, 217-
1231 230.
- 1232 Truesdell, A.H., Nathenson, M., Rye, R.O., 1977. The effects of subsurface boiling and dilution on the isotopic
1233 compositions of Yellowstone thermal waters. *J. Geophys. Res.* 82, 3694-3704.
- 1234 Tsunogai, U., Kamimura, K., Anzai, S., Nakagawa, F., Komatsu, D.D., 2011. Hydrogen isotopes in volcanic
1235 plumes: Tracers for remote temperature sensing of fumaroles. *Geochim. Cosmochim. Acta* 75, 4531-4546.
- 1236 Vacquand, C., Deville, E., Beaumont, V., Guyot, F., Sissmann, O., Pillot, D., Arcilla, C., Prinzhofer, A., 2018.
1237 Reduced gas seepages in ophiolitic complexes: Evidences for multiple origins of the H₂-CH₄-N₂ gas mixtures.
1238 *Geochim. Cosmochim. Acta* 223, 437-461.

- 1239 Valentine, D.L., Chidthaisong, A., Rice, A., Reeburgh, W.S., Tyler, S.C., 2004. Carbon and hydrogen isotope
1240 fractionation by moderately thermophilic methanogens. *Geochim. Cosmochim. Acta* 68, 1571-1590.
- 1241 Vignais, P.M., Billoud, B., 2007. Occurrence, classification, and biological function of hydrogenases: An overview.
1242 *Chem. Rev.* 107, 4206-4272.
- 1243 Von Damm, K.L., 2000. Chemistry of hydrothermal vent fluids from 9°-10°N, East Pacific Rise: "Time zero," the
1244 immediate post-eruptive period. *J. Geophys. Res.* 105, 11203-11222.
- 1245 Von Damm, K.L., Edmond, J.M., Grant, B., Measures, C.I., Walden, B., Weiss, R.F., 1985. Chemistry of submarine
1246 hydrothermal solutions at 21°N, East Pacific Rise. *Geochim. Cosmochim. Acta* 49, 2197-2220.
- 1247 Von Damm, K.L., Lilley, M.D., 2004. Diffuse flow hydrothermal fluids from 9°50'N East Pacific Rise: Origin,
1248 evolution and biogeochemical controls, in: Wilcock, W.S., Cary, C., De Long, E., Kelley, D., Barross, J. (Eds.), *The*
1249 *Subseafloor Biosphere at Mid-Ocean Ridges*, Geophys. Monogr. Ser., 144. AGU, Washington, D.C., pp. 245-268.
- 1250 Waite, J.H., Glein, C.R., Perryman, R.S., Teolis, B.D., Magee, B.A., Miller, G., Grimes, J., Perry, M.E., Miller,
1251 K.E., Bouquet, A., Lunine, J.I., Brockwell, T., Bolton, S.J., 2017. Cassini finds molecular hydrogen in the Enceladus
1252 plume: Evidence for hydrothermal processes. *Science* 356, 155-159.
- 1253 Waite, J.H., Jr., Lewis, W.S., Magee, B.A., Lunine, J.I., McKinnon, W.B., Glein, C.R., Mousis, O., Young, D.T.,
1254 Brockwell, T., Westlake, J., Nguyen, M.J., Teolis, B.D., Niemann, H.B., McNutt Jr, R.L., Perry, M., Ip, W.H., 2009.
1255 Liquid water on Enceladus from observations of ammonia and ⁴⁰Ar in the plume. *Nature* 460, 487-490.
- 1256 Walter, S., Laukenmann, S., Stams, A.J.M., Vollmer, M.K., Gleixner, G., Röckmann, T., 2012. The stable isotopic
1257 signature of biologically produced molecular hydrogen (H₂). *Biogeosciences* 9, 4115-4123.
- 1258 Wanner, C., Peiffer, L., Sonnenthal, E., Spycher, N., Iovenitti, J., Kennedy, B.M., 2014. Reactive transport modeling
1259 of the Dixie Valley geothermal area: Insights on flow and geothermometry. *Geothermics* 51, 130-141.
- 1260 Welhan, J.A., 1981. Carbon and hydrogen gases in hydrothermal systems: The search for a mantle source. PhD
1261 thesis, UC San Diego.
- 1262 Welhan, J.A., Craig, H., 1983. Methane, hydrogen and helium in hydrothermal fluids at 21°N on the East Pacific
1263 Rise in: Rona, P.A., Bostrom, K., Laubier, L., Smith, K.L., Jr. (Eds.), *Hydrothermal Processes at Seafloor Spreading*
1264 *Centers*. Plenum Press, pp. 391-409.
- 1265 White, D.E., Muffler, L.J.P., Truesdell, A.H., 1971. Vapor-dominated hydrothermal systems compared with hot-
1266 water systems. *Econ. Geol.* 66, 75-97.
- 1267 Wilcock, W.S.D., 2004. Physical response of mid-ocean ridge hydrothermal systems to local earthquakes. *Geochem.*
1268 *Geophys. Geosyst.* 5, Q110099, doi: 10.1029/2004GC000701.
- 1269 Wilmarth, W.K., Dayton, J.C., Flournoy, J.M., 1953. The mechanism of exchange of hydrogen gas and aqueous
1270 alkali. *J. Am. Chem. Soc.* 75, 4549-4553.
- 1271 Yang, H., Gandhi, H., Shi, L., Kreuzer, H.W., Ostrom, N.E., Hegg, E.L., 2012. Using gas chromatography/isotope
1272 ratio mass spectrometry to determine the fractionation factor for H₂ production by hydrogenases. *Rapid Commun.*
1273 *Mass Spectrom.* 26, 61-68.
- 1274 Yuce, G., Italiano, F., D'Alessandro, W., Yalcin, T.H., Yasin, D.U., Gulbay, A.H., Ozyurt, N.N., Rojay, B.,
1275 Karabacak, V., Bellomo, S., Brusca, L., Yang, T., Fu, C.C., Lai, C.W., Ozacar, A., Walia, V., 2014. Origin and
1276 interactions of fluids circulating over the Amik Basin (Hatay, Turkey) and relationships with the hydrologic,
1277 geologic and tectonic settings. *Chem. Geol.* 388, 23-39.

1278

1279 **FIGURE CAPTIONS**

1280 **Fig. 1.** Compendium of hydrogen isotope field data for H₂-H₂O compared with *T*-dependent equilibrium.
1281 Field data shows measured fractionation factor (α_{OBS}) vs. *T* measured during sample acquisition.
1282 Equilibrium range ($\alpha_{\text{H}_2\text{O-H}_2(\text{eq})}$, solid curves) is defined from experimental and theoretical investigations
1283 (Bardo and Wolfsberg, 1976; Horibe and Craig, 1995; Richet et al., 1977; Suess, 1949). Representative
1284 values of $\delta\text{D}_{\text{H}_2}$ (calculated assuming $\delta\text{D}_{\text{H}_2\text{O}} = -50$) are shown for reference. Alkaline springs/ophiolite
1285 data: Hakuba Happo, Japan (Suda et al., 2014); Dinaride ophiolite, Bosnia/Herzegovina (Etiope et al.,
1286 2017); Amik Basin, Turkey (Yuce et al., 2014); Semail ophiolite, Oman (Fritz et al., 1992; Miller et al.,
1287 2016; Neal and Stanger, 1983; Vacquand et al., 2018); Zambales ophiolite, Philippines (Abrajano et al.,
1288 1990; Sherwood Lollar et al., 2007; Vacquand et al., 2018). Zambales data are free gas emanations and
1289 $\delta\text{D}_{\text{H}_2\text{O}}$ and maximum measured *T* of nearby spring water are assumed (Cardace et al., 2015). Precambrian
1290 shield gases: Fennoscandian Shield, Finland (Kietäväinen et al., 2017), Gravberg, Sweden (Jeffrey and
1291 Kaplan, 1988), Canadian Shield (Sherwood Lollar et al., 2008; Sherwood Lollar et al., 2007),
1292 Witwatersrand Basin, South Africa (Onstott et al., 2006; Sherwood Lollar et al., 2007). Of shield gases,
1293 measured *T* only reported from South Africa, other values estimated using well depths and following
1294 geothermal gradient: 10 °C for top 500 m, then increasing 16 °C / km (Ahlbom et al., 1995; Jessop and
1295 Lewis, 1978; Juhlin et al., 1998; Komor et al., 1988; Marsic and Grundfelt, 2013). Datum from Lake
1296 Vida, Antarctica from Murray et al. (2012). See Figs. 8–10 for more detail and additional data references.

1297 **Fig. 2.** Schematic representation of flexible gold reaction cell system used to determine kinetics of H₂-
1298 H₂O isotope exchange (see text). Designed for hydrothermal experiments (all wetted parts are Au or Ti),
1299 time-series sampling of fluids in Au cell can be accomplished without a loss of system pressure (Seyfried
1300 et al., 1979; Seyfried et al., 1987). H₂ therefore remained fully dissolved over course of experiments.

1301 **Fig. 3.** Change in D/H composition of dissolved H₂ ($\delta\text{D}_{\text{H}_2}$) with time (*t*) at (a) 97 °C, (b) 54 °C, and (c) 22
1302 °C. Equilibrium was closely approached for all three temperatures (note *t* is normalized to zero in each
1303 panel relative to total duration of experiment (Table 1). Experimental data were fit with an exponential
1304 function of form $y = y_0 + Ae^{-x/B}$, where asymptote is y_0 , or expected equilibrium value ($\delta\text{D}_{\text{H}_2(\text{eq})}$, reported
1305 uncertainties are 95% confidence intervals). These values were used to derive respective rate constants
1306 (Fig. 4), and to compare results with predicted equilibrium values (Fig. 7). Values of $\delta\text{D}_{\text{H}_2(\text{eq})}$ calculated
1307 using two different *T* vs. $\alpha_{\text{H}_2\text{O-H}_2(\text{eq})}$ relationships (see also section 4.2, Fig. 7) and the experimental $\delta\text{D}_{\text{H}_2\text{O}}$
1308 value (+5220 ‰) shown for comparison (dashed lines).

1309 **Fig. 4.** Experimental data cast in form of fractional approach to equilibrium with time (*t*) at (a) 97 °C, (b)
1310 54 °C, and (c) 22 °C (see equations 8, 9). Slope of linear regressions yield rate constants (k_1 , in hrs⁻¹),
1311 where dashed lines and reported uncertainty in k_1 both represent 95% confidence. All three regressions
1312 were forced to intercept origin, though data at 97 and 54 °C did so naturally within uncertainty. Data for *t*
1313 > 245 hrs in the 97 °C experiment are not included in the regression because the measured $\delta\text{D}_{\text{H}_2}$ values
1314 are at or beyond the extrapolated equilibrium value within analytical reproducibility (cf Table 1, Fig. 3).

1315 **Fig. 5.** Arrhenius plot depicting *T* dependence of rate constants (k_1) derived in Fig. 4. A weighted linear
1316 regression of new experimental data yields: $\ln k_1 = 13.0 (\pm 0.2) - 6238 (\pm 61) / T$ (2 σ uncertainty) with R²

1317 = 0.9998. Dashed lines represent 95% confidence interval. Slope gives activation energy (E_a) of 51.9
1318 kJ/mol. Literature data shown for comparison were not included in regression (see section 4).

1319 **Fig. 6.** Arrhenius style plots showing density-based rate model for D–H exchange between H_2 and H_2O .
1320 Panel (a) shows data from present study, and those recast from Lecluse and Robert (1994), where both
1321 datasets are "normalized" to system density of 1 mol/L (see section 4.1). Historical data points represent
1322 average of 11 ($\ln k = -7.12 \pm 1.11$), 15 ($\ln k = -4.61 \pm 3.04$), 10 ($\ln k = -1.86 \pm 2.71$), and 4 ($\ln k = 0.48 \pm$
1323 3.65) individual batch experiments conducted at 100, 200, 300 and 400 °C, respectively, and error bars
1324 are 2σ . A weighted regression of combined data sets gives: $\ln k$ (in [L/mol] / hr) = $9.186 (\pm 0.18) - 6297$
1325 $(\pm 63) / T$ (2σ uncertainty), where dashed lines represent 95% prediction limit, and associated $E_a = 52.4 \pm$
1326 1.3 kJ/mol (95% CI). Panel (b) presents effective first order k_1 values (hr^{-1}) for both experimental datasets.
1327 Stand-alone regression of k_1 values from Lecluse and Robert (1994) gives $E_a = 48 \pm 14$ kJ/mol (95% CI),
1328 consistent with other regressions (above and Fig. 5) despite higher uncertainty. Experimental data are
1329 compared with calculated k_1 values (using equation 17) along vapor and liquid curves of pure H_2O (star is
1330 critical point), and also a high pressure isobar (10,000 bars). The latter demonstrates how
1331 incompressibility of liquid water should result in less variability in isotope exchange rate relative to vapor
1332 phases.

1333 **Fig. 7.** Equilibrium isotope (D/H) fractionation between H_2O and H_2 ($\alpha_{H_2O-H_2(eq)}$) as a function of T .
1334 Experimental $\alpha_{H_2O-H_2(eq)}$ values are calculated as $(\delta D_{H_2O(eq)} + 10^3) / (\delta D_{H_2(eq)} + 10^3)$ using data from Fig. 3
1335 and $\delta D_{H_2O(eq)} = +5220 \pm 50$ ‰ (2σ). This yields 2.605 ± 0.024 (97 °C), 3.126 ± 0.028 (54 °C), and $3.814 \pm$
1336 0.070 (22 °C). Compared are equilibrium curves for gaseous H_2 coexisting with liquid H_2O ($\alpha_{H_2O(L)-H_2(g)}$)
1337 and H_2O vapor ($\alpha_{H_2O(v)-H_2(g)}$). New data was used in defining $\alpha_{H_2O(liq)-H_2(aq)}$ or $\alpha_{H_2O(L)-H_2(AQ)}$ (solid line),
1338 along with values calculated using $\alpha_{H_2O(L)-H_2(g)}$ and corresponding $\alpha_{H_2(aq)-H_2(g)}$ values taken from Knox et al.
1339 (1992), Muccitelli and Wen (1978) and Symons and Buncel (1973). Estimated uncertainties for these data
1340 are given in legend for clarity. Note $\alpha_{H_2O(v)-H_2(g)}$ and $\alpha_{H_2O(L)-H_2(g)}$ are comparable to relationship given by
1341 Bardo and Wolfsberg (1976), and equation 8 of Horibe and Craig (1995), respectively, in T range shown.
1342 The three $\alpha_{H_2O-H_2(eq)}$ curves may be calculated using coefficients given in Table 2. See section 4.2 and
1343 Supplementary Information for derivation.

1344 **Fig. 8.** a) Measured α_{OBS} vs. measured sampling T in deep-sea (black smoker) hydrothermal fluids
1345 (Kawagucci, 2015; Kawagucci et al., 2011; Kawagucci et al., 2016; Kawagucci et al., 2010; Konn et al.,
1346 2018; Proskurowski et al., 2006; Welhan and Craig, 1983), compared with equilibrium fractionation
1347 ($\alpha_{H_2O(L)-H_2(AQ)}$, see Fig. 7, Table 2) and a kinetic fractionation trend assuming a cooling rate of 50 °C / hr
1348 (dashed). Panel (b) demonstrates how subsurface mixing between high- T hydrothermal end-member and
1349 seawater accounts for lower measured temperatures, which quenches isotopic re-equilibration more
1350 rapidly than conductive cooling. Mixing should not affect α_{OBS} because δD_{H_2O} of vent fluids and seawater
1351 are equivalent (Shanks, 2001). Trend of increasing α_{OBS} for $T < \sim 60$ °C is likely biologically influenced
1352 (see section 4.4.1). Alpha values measured in seafloor sediment pore fluids shown for comparison (Toki
1353 et al., 2011).

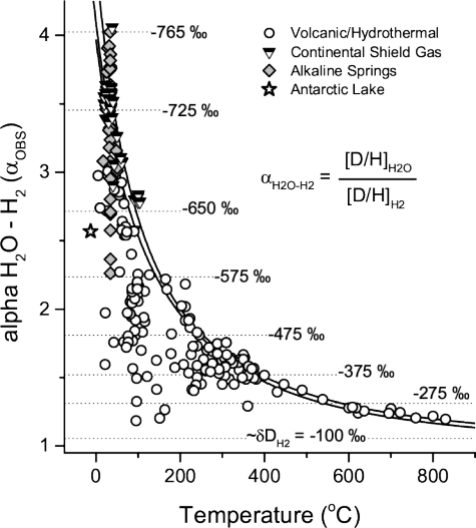
1354 **Fig. 9.** Measured α_{OBS} vs. measured sampling T in hydrothermal fluids from Lost City vent field
1355 (Proskurowski et al., 2006), compared with equilibrium fractionation ($\alpha_{H_2O(L)-H_2(AQ)}$, see Fig. 7, Table 2),
1356 and respective kinetic fractionation trends (dashed) fit to group 1 fluids having higher δD_{H_2} and dissolved
1357 H_2 , and $T > 65$ °C (see inset and section 4.4.2). Though not appreciably different, T reported here are

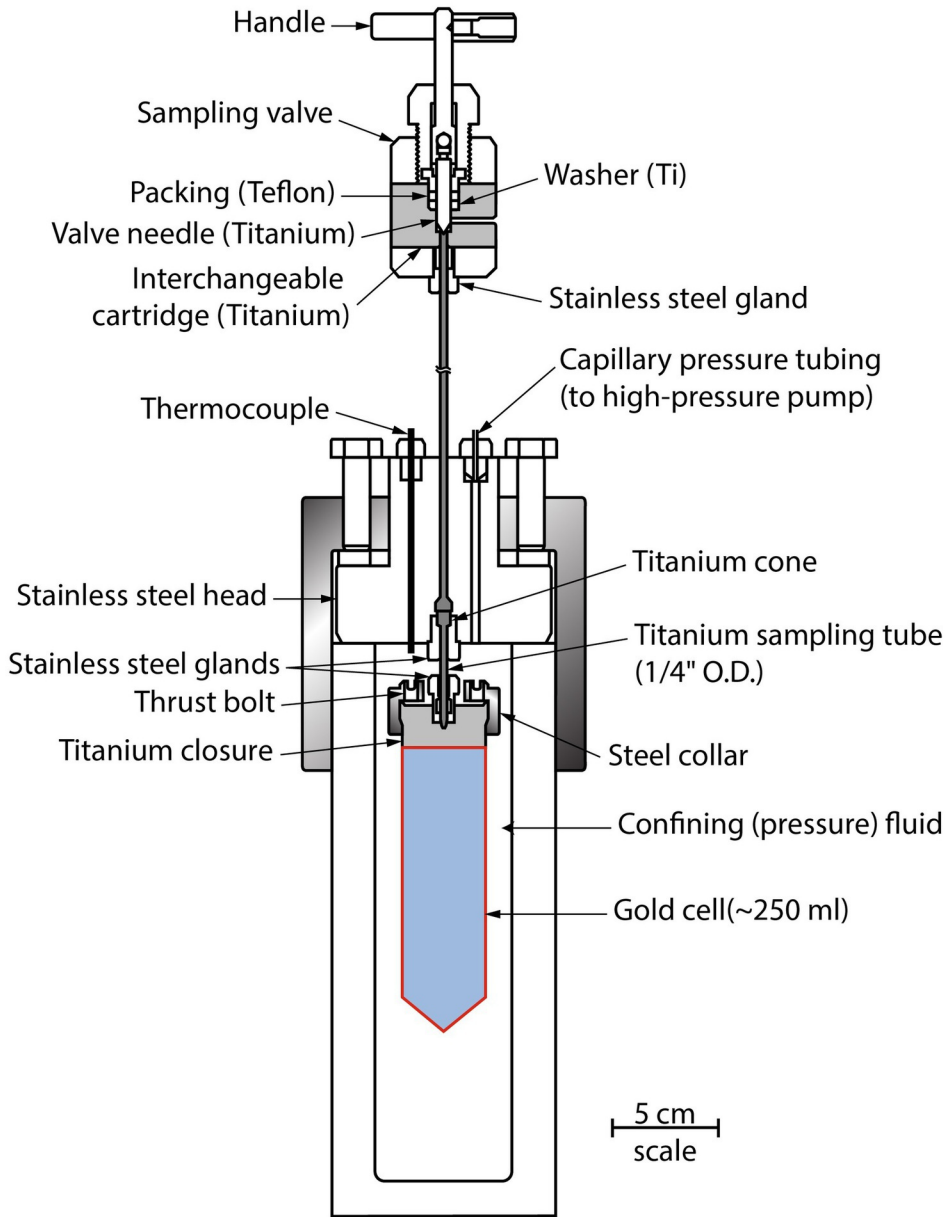
1358 maximum values from each vent site (Lang et al., 2012) to better account for ambient seawater
1359 entrainment during sampling of more diffuse fluids. Kinetic models assumed isotopic equilibrium at 250
1360 °C, and results indicate fluids were still near equilibrium at 190 °C, the apparent T of last fluid–mineral
1361 equilibration (star symbol, after Seyfried et al., 2015). Group 2 fluids suggest biologically enhanced rates
1362 of isotopic equilibration.

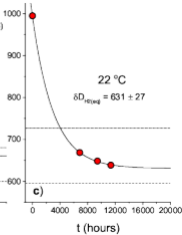
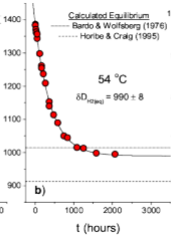
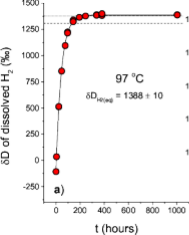
1363 **Fig. 10.** Measured α_{OBS} vs. measured sampling T from variety of continental volcanic/geothermal settings,
1364 compared with $\alpha_{\text{H}_2\text{O(L)}-\text{H}_2\text{(AQ)}}$ equilibrium fractionation ($\alpha_{\text{H}_2\text{O(v)}-\text{H}_2\text{(g)}}$ may be more relevant to
1365 fumarole/steam samples, but differs little from $\alpha_{\text{H}_2\text{O(L)}-\text{H}_2\text{(AQ)}}$ over T region shown). Note log T scale.
1366 Example kinetic fractionation trends (dashed) are shown for reference, and parentheses indicate how T -
1367 ρ_{W} dependence was constrained (S. Vap and S. Liq are densities along vapor and liquid branch of H_2O
1368 steam saturation curve). Data from Yellowstone (14 °C / hr model fit) are highlighted for discussion (see
1369 text). Data sources by locality: Iceland (Arnason, 1977; Arnason and Sigurgeirsson, 1968), Japan
1370 (Kiyosu, 1983; Kiyosu and Okamoto, 1998; Mizutani, 1983; Tsunogai et al., 2011), Socorro Island (Taran
1371 et al., 2010), Kamchatka (Taran et al., 1992), Greece, shallow Aegean Sea (Botz et al., 1996),
1372 Yellowstone (Gunter and Musgrave, 1971; Welhan, 1981), New Zealand (Lyon and Hulston, 1984). Of
1373 New Zealand samples, measured T not reported for geothermal wells at Wairakei, nor Broadlands,
1374 isotopic values were therefore averaged and plotted against known reservoir temperatures, 255 and 290
1375 °C, respectively (Glover and Mroczek, 2009; Simmons et al., 2016). Arrows connect data from Ngawha
1376 wells (NZ) and associated surface pools (see section 4.5).

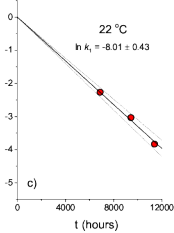
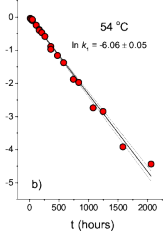
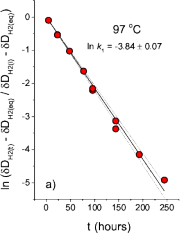
Table 1.					
Experimental change in δD_{H_2} (VSMOW) of dissolved H_2 with time (t)					
t (hrs) ^a	δD_{H_2} (‰)	Δt (days) ^b	t (hrs)	δD_{H_2} (‰)	Δt (days)
<i>97 °C and 70 bars</i>			<i>54 °C and 70 bars</i>		
0.0	-106.7		0.0	1383.1	18
4.5	35.0		0.0	1386.4	181
22.8	511.7	6	3.7	1383.3	
22.8	514.0	611	14.7	1371.2	
47.8	853.2		27.5	1360.4	17
77.1	1095.6		27.5	1363.2	180
95.6	1224.6	3	47.1	1344.2	16
95.6	1215.1	17	47.1	1357.0	179
143.6	1336.9	1	114.6	1297.7	
143.6	1323.2	15	163.6	1261.4	11
192.6	1364.5		163.6	1254.5	174
244.6	1377.1		209.0	1236.6	
335.6	1389.9	7	261.5	1209.0	
335.6	1383.6	598	360.7	1152.8	166
381.8	1383.3	5	360.7	1139.6	555
381.8	1399.5	44	474.4	1113.7	
1004.8	1390.0	18	578.1	1089.7	
1004.8	1388.0	181	740.6	1050.2	
<i>22 °C and 70 bars</i>			835.7	1044.8	
0.0	990.0		1078.0	1015.4	
6864.0	668.4		1244.4	1012.9	
9432.0	648.2		1580.3	997.8	
11376.0	638.6		2061.0	994.7	
a) time normalized for each temperature					
b) time between sampling and analysis, demonstrates no meaningful change in δD_{H_2} during sample storage					

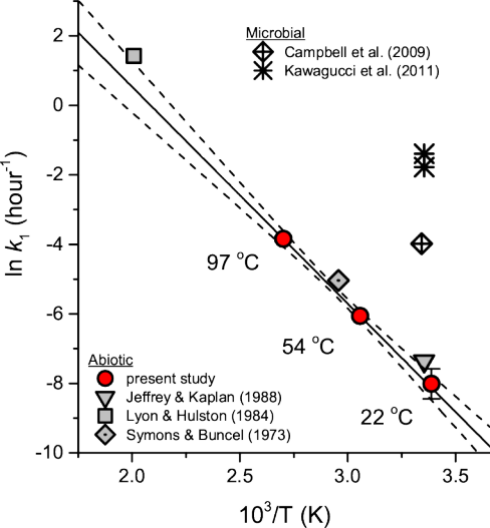
Table 2.			
Polynomial coefficients for equilibrium D/H fractionation ^{a,b} in the water-hydrogen system: $\alpha_{\text{H}_2\text{O}-\text{H}_2(\text{eq})} = A + B/T^2 + C/T^4 + D/T^6$			
$\alpha_{\text{H}_2\text{O}-\text{H}_2(\text{eq})}$	$\text{H}_2\text{O}_{(\text{vap})} / \text{H}_2(\text{g})$ $(\alpha_{\text{H}_2\text{O}(\text{v})-\text{H}_2(\text{g})})$	$\text{H}_2\text{O}_{(\text{liq})} / \text{H}_2(\text{aq})$ $(\alpha_{\text{H}_2\text{O}(\text{L})-\text{H}_2(\text{AQ})})$	$\text{H}_2\text{O}_{(\text{liq})} / \text{H}_2(\text{g})$ $(\alpha_{\text{H}_2\text{O}(\text{L})-\text{H}_2(\text{g})})^c$
A	0.9997	1.00138	1.01847
B	218170	219788	200833
C	-2.056E+08	-2.926E+09	2.899E+09
D	8.315E+13	4.108E+14	1.289E+14
a) input is absolute T (K)			
b) regression statistics given in Supplementary Information			
c) assumes H_2O liquid and vapor coexist, $0 \leq T < 374$ °C			

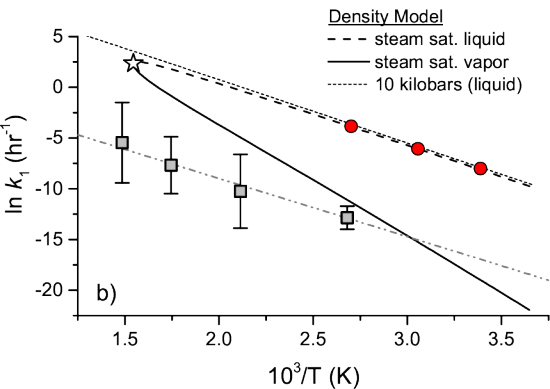
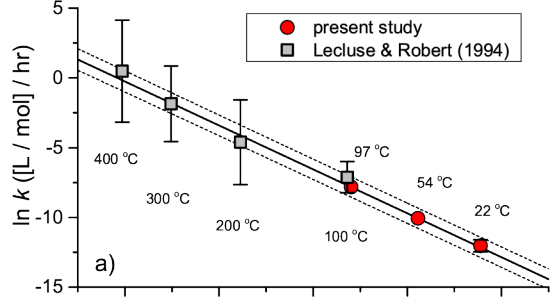


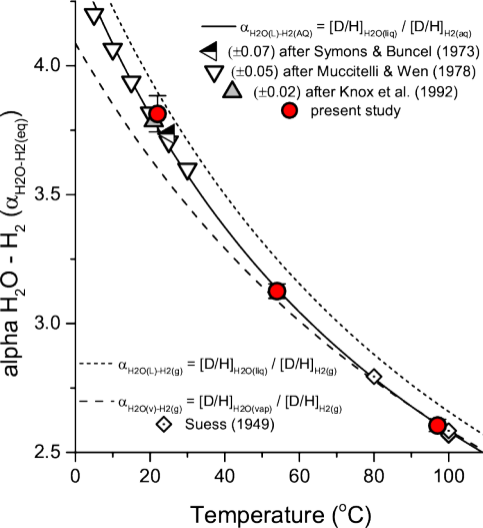


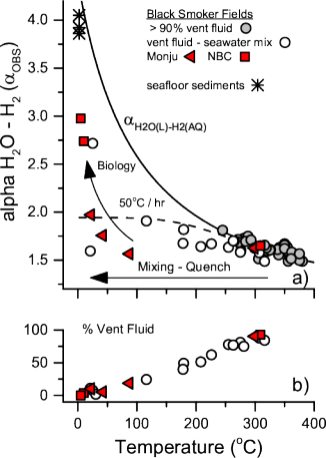


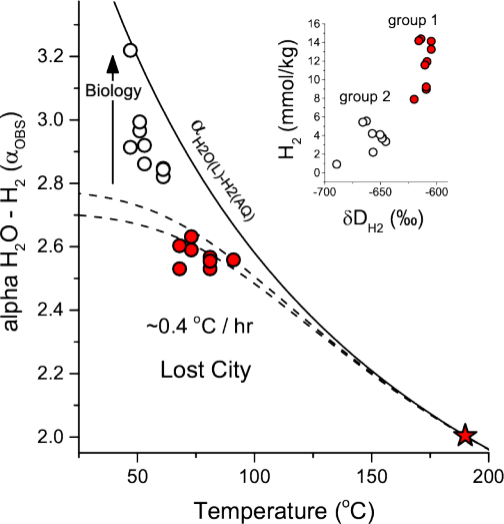












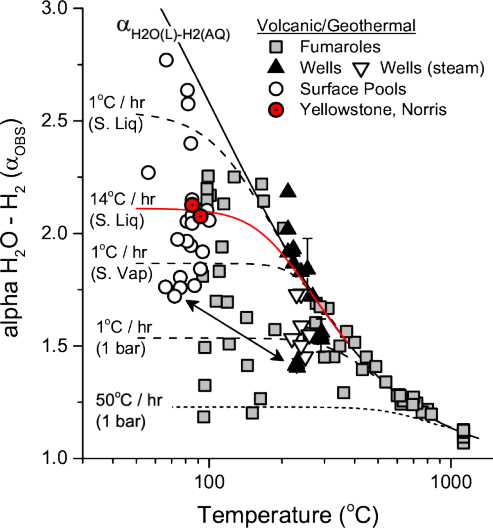


Table 1.

Experimental change in δD_{H_2} (VSMOW) of dissolved H_2 with time (t)

t (hrs) ^a	δD_{H_2} (‰)	Δt (days) ^b	t (hrs)	δD_{H_2} (‰)	Δt (days)
<i>97 °C and 70 bars</i>			<i>54 °C and 70 bars</i>		
0.0	-106.7		0.0	1383.1	18
4.5	35.0		0.0	1386.4	181
22.8	511.7	6	3.7	1383.3	
22.8	514.0	611	14.7	1371.2	
47.8	853.2		27.5	1360.4	17
77.1	1095.6		27.5	1363.2	180
95.6	1224.6	3	47.1	1344.2	16
95.6	1215.1	17	47.1	1357.0	179
143.6	1336.9	1	114.6	1297.7	
143.6	1323.2	15	163.6	1261.4	11
192.6	1364.5		163.6	1254.5	174
244.6	1377.1		209.0	1236.6	
335.6	1389.9	7	261.5	1209.0	
335.6	1383.6	598	360.7	1152.8	166
381.8	1383.3	5	360.7	1139.6	555
381.8	1399.5	44	474.4	1113.7	
1004.8	1390.0	18	578.1	1089.7	
1004.8	1388.0	181	740.6	1050.2	
<i>22 °C and 70 bars</i>			835.7	1044.8	
0.0	990.0		1078.0	1015.4	
6864.0	668.4		1244.4	1012.9	
9432.0	648.2		1580.3	997.8	
11376.0	638.6		2061.0	994.7	

a) time normalized for each temperature

b) time between sampling and analysis, demonstrates no meaningful change in δD_{H_2} during sample storage

Table 2.

Polynomial coefficients for equilibrium D/H fractionation^{a,b} in the water-hydrogen system: $\alpha_{\text{H}_2\text{O}-\text{H}_2(\text{eq})} = A + B/T^2 + C/T^4 + D/T^6$

$\alpha_{\text{H}_2\text{O}-\text{H}_2(\text{eq})}$	$\text{H}_2\text{O}_{(\text{vap})} / \text{H}_2(\text{g})$ ($\alpha_{\text{H}_2\text{O}(\text{v})-\text{H}_2(\text{g})}$)	$\text{H}_2\text{O}_{(\text{liq})} / \text{H}_2(\text{aq})$ ($\alpha_{\text{H}_2\text{O}(\text{l})-\text{H}_2(\text{aq})}$)	$\text{H}_2\text{O}_{(\text{liq})} / \text{H}_2(\text{g})$ ($\alpha_{\text{H}_2\text{O}(\text{l})-\text{H}_2(\text{g})}$) ^c
A	0.9997	1.00138	1.01847
B	218170	219788	200833
C	-2.056E+08	-2.926E+09	2.899E+09
D	8.315E+13	4.108E+14	1.289E+14

a) input is absolute T (K)

b) regression statistics given in Supplementary Information

c) assumes H_2O liquid and vapor coexist, $0 \leq T < 374$ °C